JAMES RENNELL CENTRE FOR OCEAN CIRCULATION

INTERNAL DOCUMENT No. 11

Analysis of meteorological data from RRS *Charles Darwin* Cruises CD46 & CD47 (BOFS Experiment)

R J Tiddy, R W Pascal, K G Birch & P K Taylor

1993

Chilworth Research Park
Chilworth
Southampton SO1 7NS
Tel 0703 766184
Telefax 0703 767507

DOCUMENT DATA SHEET

AUTHOR
R.J.Tiddy, R.W.Pascal, K.G.Birch, P.K.Taylor

PUBLICATION DATE
March 1991

TITLE
Analysis of meteorological data from *RRS Charles Darwin* cruises CD46 and CD47 (BOFS experiment)

REFERENCE
James Rennell Centre for Ocean Circulation Internal Document No. 11, 57pp

ABSTRACT

The IOSDL MultiMet meteorological instrumentation system was used during the BOFS experiment on *RRS Charles Darwin* cruises 46 and 47. This report describes and evaluates the quality of the meteorological data obtained. Recommendations for using the data include a 0.45°C correction to the forward dry bulb temperature and the use of wind directions from the main mast wind vane rather than the foremast propellor-vane. The temperature difference between the foremast and wheelhousetop psychrometer measurements was found to be a function of solar radiation and wind speed. A model of this effect was developed. From anemometer comparisons acceleration of the air flow over the ship was estimated to be 4%. The solar radiation sensors agreed to within a few W/m^2 except for anomalous values on two days.

KEYWORDS

RRS Charles Darwin
cruises CD46 and CD47

BOFS
Air Sea Fluxes

ISSUING ORGANISATION

Jame Rennell Centre for Ocean Circulation
Chilworth Research Park
Chilworth, SOUTHAMPTON, U.K.

(Part of IOSDL)
Director: Colin Summerhayes DSc

Telephone Wormley (0428) 684141
Telex 858833 Oceans G.
Facsimile (0428) 683066

Copies of this report are available from: ***The Library,IOSDL.***

PRICE

CONTENTS **Page**

1. INTRODUCTION

The aim of this report is to describe and evaluate the quality of the meteorological data for the BOFS (Biogeochemical Ocean Flux Survey) experiment from *RRS Charles Darwin* cruises CD 46 (28th April to 22nd May 1990, day number 118 to 142), and CD 47 (25th May to 17th June 1990, day number 145 to 168).

The next section will describe the sensors used and their calibration; section 3 presents the time series data, and discusses the editing required for the removal of spikes. Section 4 investigates the quality of the temperature data, considering the errors in the psychrometers and the corrections needed to overcome these biases, and the effects of funnel exhaust on the psychrometers with respect to wind direction. The difference between the temperature data from the forward mast and the starboard and port psychrometers is shown to be dependent on insolation, wind speed and relative wind direction. To further analyse this difference a statistical investigation of correlation was performed between one dependent variable (temperature difference between the dry bulb starboard psychrometer and the dry bulb forward psychrometer) and three independent variables: shortwave radiation, wind velocity and wind direction. Section 5 quantifies the errors in the anemometer readings due to the different heights of the anemometers on the forward and main masts. Section 6 compares the short wave solar radiation data between the starboard and port sensor. The conclusions are summarised in section 7. Appendix I describes in more detail the statistical analysis presented in section 4. Appendix II shows the calibration certificates for the psychrometers and anemometers.

2. SENSORS

2.1 Sensor Positions

The sensors were situated on the forward mast, main mast, and on the port and starboard side of the wheelhousetop (figure 1a). The forward mast (figure 1b) carried a propeller vane anemometer (R.M.Young serial number (S/N) 6692) situated on the forward platform, 1 metre to port of the upper foremast and 2.6 metres above the platform (approximately 15 metres above the sea). An aspirated psychrometer (Vector instruments (VI) S/N 1066) was situated just below and forward of the anemometer. The short wave radiation sensors were situated to the far port and starboard side of the forward mast platform (Kipp and Zonnen S/N 1058 and 0607). The long wave radiation sensor (Eppley S/N 6207) was situated at the top of the upper foremast. On the wheelhousetop there was an aspirated psychrometer (VI S/N 1071) situated to the port side, and also to the starboard side (VI S/N 1070), in each case just aft of the ladder and approximately 1.8 metres above the deck. The main mast carried an anemometer (VI S/N 1892) and a wind direction sensor (VI S/N 2118) situated at the mast top.

2.2 Sensor Calibration

Wind direction and wind velocity sensors were calibrated by IOSDL staff at the Bracknell Meteorological Office wind tunnel; the manufacturers calibration was used for the solar radiation sensors; psychrometers were calibrated in the IOSDL temperature bath both before and after the cruise. Table 1 gives the calibration coefficients based on the pre-cruise calibration:

Table 1: Pre Cruise Calibration Coefficients

VARIABLE	CHANNEL	C(1)	C(2)	C(3)	C(4)
LW	(1)	233.6450	0		
SW_S	(2)	206.6120	0		
SW_P	(3)	221.2390	0		
DD_{FM}	(4)	72	0		
TW_S	(5)	-20.2983	-1.9838E-4	9.6322E-6	3.5245E-10
TD_S	(6)	-21.0918	-1.5693E-4	8.9877E-6	3.0117E-10
TW_P	(7)	-21.2974	1.6523E-3	8.6580E-6	4.9633E-10
TD_P	(8)	-20.9362	8.2597E-4	8.3806E-6	4.3652E-10
TW_{FM}	(9)	-20.1399	3.4150E-4	9.1004E-6	4.2651E-10
TD_{FM}	(10)	-21.5903	1.4466E-3	8.1250E-6	4.2651E-10
SST	(11)	-1776.4715	2.7979	-1.4863E-3	2.7145E-7
VV_{FM}	(12)	1.1982	0		
VV_{MM}	(13)	0.0980	0		
DD_{MM}	(14)	1	0		
DD_{SHIP}	(15)	1	0		

Where: LW = *long wave solar radiation,* SW_S = *starboard short wave radiation,* SW_P = *port short wave radiation,* DD_{FM} = *wind direction from the forward mast sensor,* TW_S = *starboard wet bulb temperature,* TD_S = *starboard dry bulb temperature,* TW_P = *port wet bulb temperature,* TD_P = *port dry bulb temperature,* TW_{FM} = *forward mast wet bulb temperature,* TD_{FM} = *forward mast dry bulb temperature,* SST = *sea surface temperature,* VV_{FM} = *wind speed from the forward mast sensor,* VV_{MM} = *wind speed from the main mast sensor,* DD_{MM} = *wind direction from the main mast sensor,* DD_{SHIP} = *ships heading.*

The calibration details for the psychrometers and anemometers are listed in Appendix II and contain pre-cruise and post-cruise figures for both instruments. These calibration coefficients are used in the following equations (where g = geophysical value, *s* = sensor value):

A. Analogue channels (channel numbers: 1, 2, 3, 4)
g=((8190-s)/819)*C(1)

B. frequency channels temperatures (channel numbers: 5, 6, 7, 8, 9, 10, 11)
g=C(1)+s*C(2)+s*C(2)+s*C(3)+s*C(4)

C. frequency channels wind speeds (channel numbers: 12, 13)
g=s*0.02*C(1)+C(2)

D. Digital channels directions (channel numbers: 14, 15)
g=s*C(1)+C(2)

Using pre and post-cruise calibrations, the air temperature differences were found to be negligibly small (Appendix II). Differences in pre and post-cruise wind speeds for the Young anemometer on the forward mast were also found to be small; but significant differences were found for the anemometer on the main mast. This will be discussed further in section 5.

2.3 Thermometer calibration correction

Following the cruise it was discovered that the standard thermometer, used as a calibration standard for the thermometers, was programmed with the wrong calibration coefficients. The error (Table 2) amounts to about 0.2°C to 0.3°C for the range of temperatures experienced during the BOFS cruises. The correction formula is:

$$T_{corr} = 0.00247\ (T_{calc})^2 + 0.9757\ (T_{calc}) - 0.0271$$

Where T_{corr} is the correct value (°C) and T_{calc} the value calculated with the incorrect standard thermometer calibration. This correction has been applied to the data files for these cruises, however it had not been applied when Figures 2 and 3 were produced. The reported comparisons between different thermometers will not be significantly in error since all thermometers had been calibrated to the same standard.

Table 2. Correction values to allow for the error in the standard thermometer.

T_{corr} (°C)	Correction (°C)
0	-0.03
5	-0.14
10	-0.25
15	-0.34
20	-0.41
25	-0.48
30	-0.53

3. TIME SERIES DATA

3.1 Introduction

Figures 2 and 3 are plots of all the variables against the day number (JDAY) for cruises CD 46 and CD 47 respectively. These data have been 'despiked' (section 3.2). The plots show successive 5 day intervals. Figures 2a, c, e, etc. show the wind direction from the main mast and forward mast and the corresponding relative wind speeds. The normal practice is to mount the wind vanes with 180° orientated to the ships bow to minimise occurrence of 0° to 360° changes in record. However for these cruises the Young propeller vane anemometer on the forward mast was inadvertently mounted with 0° towards the ships bow. Since this is logged on a conventional analogue channel, erroneous wind directions will have occured due to averaging signals on either side of 360°. In contrast the Vector Instruments wind vane on the main mast was mounted with 180° toward the bow, and specially sampled to avoid incorrect averaging (Birch and Pascal, 1987). Thus the main mast wind directions should be used in preference to those from the foremast. The wind speed data will be compared later (section 5).

Figures 2b, d, f, etc. show the radiation data, and the wet and dry bulb temperatures from the forward mast and wheelhouse top screens. Both port and starboard radiation sensor data are plotted, however on the scale shown these are normally indistinguishable (see section 6 for comparisons). The sea surface temperature data, where present, is superimposed on the forward mast temperature plot. These SST data were collected between day number 125 to 141 for CD 46, and between day numbers 160 to 165 on CD 47, although then only for short periods to the end of the cruise.

3.2 Despiking

The data originally had 'spikes' within it; probably caused by radio frequency interference. These have been removed using the pstar program, DSPIKE. An example can be seen in Figure 4 of the original LW (long wave radiation) for CD 47 with spikes; and the 'despiked' longwave data in Figure 5. Although some small spikes remain the major errors have been removed.

Table 3 shows the number of spikes removed for the relevant variables for CD46 and CD47 respectively. For any one variable, the maximum number of data records removed was 210 for CD 46 out of an original 32793, and 174 for CD 47 out of an original 31567 (without taking into account sea surface temperature, which has exceptionally large number of missing or poor data values).

Table 3: Number of Spikes Removed

VARIABLE	NO.SPIKES	NO.SPIKES
(see Table1 for key)	CD 46	CD 47
LW	120	40
TW_S	210	20
TD_S	11	0
TW_P	11	0
TD_P	11	91
TW_{FM}	12	0
TD_{FM}	14	174
SST	379	3616

Inspection of the original data plots indicated that the remaining variables did not require editing.

4. QUALITY OF TEMPERATURE DATA

4.1 Introduction

The psychrometer on the forward mast is well exposed for most wind directions, those on the wheelhouse top are likely to be sheltered for some relative wind directions and more effected by heat from the ship. Thus the forward mast psychrometer should normally be used to define the air temperature. However in view of the need to correct the dry bulb reading from that psychrometer (section 4.2), comparison between the different psychrometer readings is considered worthwhile. The results will also be of interest when using data from ships with less well exposed psychrometers or screens. Cruise CD 47 data will be used for this comparison.

Assuming a correctly calibrated psychrometer, there are two major potential sources of temperature error: heat from the ships engines and ventilation system, and solar radiation both by heating the psychrometers directly and, indirectly, through heating of the ships deck and superstructure.

4.2 Psychrometer Calibration Errors

In order to compare the readings from the different psychrometers the night time temperature data has been examined for cases where the ship was head to wind (ie. relative wind direction between 330 and 30 degrees, Figure 6). For these cases differences due to solar radiation and poor sensor exposure should be negligible and each sensor would on

average be expected to give the same reading. Table 4 shows the mean temperature and humidity differences for CD 46 and CD 47.

Table 4: CD 46 and CD 47 Mean Temperature Differences and Resulting Humidity Differences

	CD 46			CD 47		
	N	M (^{o}C)	S.D	N	M (^{o}C)	S.D
TD_{FM}-TD_{P}	9252	0.463	0.0005	7884	0.450	0.0008
TD_{FM}-TD_{S}	9252	0.442	0.0005	7884	0.399	0.0010
TW_{FM}-TW_{P}	9252	0.007	0.0006	7884	-0.057	0.0009
TW_{FM}-TW_{S}	9252	-0.025	0.0004	7884	-0.050	0.0007
Q_{FM}-Q_{P}	9252	-0.187	0.0083	7884	-0.246	0.0011
Q_{FM}-Q_{S}	9252	-0.210	0.0004	7884	-0.218	0.0007

Where:N = *number of data points* M = *mean value*
S.D = *standard deviation* Q = *Specific humidity at relevant position*
And the other variable notation as is used in Table 1.

Compared to the port and starboard psychrometers the forward dry bulb temperature read high by about 0.45°C, and was corrected accordingly. The calibration certificates for the psychrometers (showing pre-cruise and post-cruise figures), show no significant changes in calibration for the period of deployment (Appendix II). Therefore the discrepancy of dry bulb temperatures on the foremast can not be accounted for by means of shift in the calibration. It is possible that the frequency signal might have been miscounted at the logger, resulting in a lower value of temperature being recorded. The change in this error during the cruises showed a systematic trend (Figure 7), however the overall changes were negligible (<0.1°C).

The validity of applying a 0.45°C correction to the forward dry bulb can be checked by recalculating the specific humidity differences. Table 5 shows the differences between the forward, port and starboard humidities for CD 46 and CD 47. Compared to values shown in Table 4, the specific humidity differences were much reduced as is expected (as the specific humidity is conserved over the ship), therefore confirming the temperature correction.

Table 5: CD 46 and CD 47 Recalculated Mean Specific Humidity Differences after Temperature Correction

	CD 46			CD 47		
	N	M (g/Kg)	S.D	N	M (g/Kg)	S.D
Q_{FM}-Q_{P}	32579	-0.043	5.2*10-4	31372	-0.090	$6.2*10^{-4}$
Q_{FM}-Q_{S}	32579	-0.035	3.5*10-4	31372	-0.040	$4.1*10^{-4}$

(For key, see Table 4)

4.3 Heat from Ship

Figure 8 shows the difference in dry bulb temperature reading, ΔT, between each of the wheelhouse top psychrometers and that on the foremast. The data from the whole of Cruise 47 has been averaged for each ten degree relative wind direction sector. The effect of funnel smoke shows up clearly for the starboard psychrometer, ΔT_S (= T_S-T_{FM}) for relative wind directions of 200° to 250°, corresponding to the funnel being downwind of the psychrometer. This effect is not clearly seen for the port psychrometer, ΔT_P (= T_p-T_{FM}). The reason for this is not known.

4.4 Solar heating

4.4.1 Diurnal Variation of Temperature Differences

Figure 9 shows the mean diurnal variation of downward shortwave radiation during Cruise 47. The maximum occurs at about 1300 gmt (corresponding to noon local solar time). No phase shift can be seen between the peak of the mean diurnal temperature differences ΔT_S, ΔT_P, and the peak of the mean diurnal short wave radiation.

The temperature difference, ΔT_S, is shown in Figure 10 as a function of the incoming shortwave radiation. ΔT_S increases rapidly above 250W/m^2. However at high incoming radiation values there is a decrease. This is explained by Figure 11, which shows that ΔT_S is also a function of relative wind speed, and Figure 12 which shows that on average the occasions of high solar radiation corresponded, on Cruise 47, to a higher relative wind.

4.4.2 Dependence on Radiation and Wind Speed

A mathematical analysis was undertaken to explain how the temperature difference between the dry bulb starboard psychrometer and the dry bulb forward psychrometer is related to the wind speed and the shortwave solar radiation. Assume:

$$\Delta T_S = \text{function (VV, RS)} \qquad (1)$$

where: ΔT_S = dry starboard temperature - dry forward temperature, VV = wind velocity on the forward mast, RS = short wave solar radiation on the starboard sensor

The required function can be investigated using the following two partial derivatives:

$$\partial \Delta T_S / \partial VV \quad \text{where RS is constant} \qquad (i)$$

$$\partial \Delta T_S / \partial RS \quad \text{where VV is constant} \qquad (ii)$$

To investigate the dependence of ΔT on VV (partial derivative (i)) the data set for CD 47 was divided into cases of low, medium and high solar radiation, where:

a) RS lay between 0 and 200 W/m^2
b) RS lay between 200 and 400 W/m^2
c) RS lay between 400 and 600 W/m^2

Regression plots (Figure 13a) of the temperature difference against wind speed for a,b,c resulted in three different linear regression equations, of the form:

$$\Delta T_s = mVV + c \qquad (2)$$

where: m = gradient, c = y intercept (function of RS)

Figure 13a shows for high values of solar radiation, there is a large change in temperature difference with wind speed. For low solar radiation, there is a much smaller change in temperature difference with wind speed.

The gradients (m) were then plotted against the three mean values of solar radiation (ie: 100, 300, 500,) a linear relationship was found (Figure 14) of the form:

$$m = gRS + h \qquad (3)$$

back substitution in equation 2 gives:

$$\Delta T_s = (gRS + h)VV + c \qquad (4)$$

The modulus of c (function of RS) is negligible compared to the modulus of the other variables, therefore the mathematical model shows that the temperature difference is caused by the direct effect of radiation, with a modification to take into account the relative wind. This model explained 17.6 % of the variance:

$$\Delta T_s = gVVRS + hVV \qquad (5)$$

where if in equation 5: RS is measured in W/m^2, VV is measured in m/s, and ΔT_s is measured in °C; then: $g \approx -0.0002$, $h \approx 0.0014$

To investigate the dependence of ΔT on RS (partial derivative (ii)) the data set for CD 47 was divided into cases of low, medium, and high wind speed, where:

d) VV lay between 0 and 5 m/s
e) VV lay between 5 and 10 m/s
f) VV lay between 10 and 16 m/s

Regression plots (Figure 13b) of the temperature difference against solar radiation for d,e,f resulted in three different linear regression equations, of the form:

$$\Delta T_s = mRS + c$$

The gradients (m) were then plotted against the three mean values of wind speed (ie: 2.5, 7.5, 13). The relationship is non linear (Figure 15).

4.4.3 Statistical Model

A further indication of the importance of the two terms on the right hand side of equation 5 was obtained by the statistical analysis of starboard sensor data for BOFS 47, which investigated the correlation between one dependent variable (temperature difference between the dry bulb starboard psychrometer and the dry bulb forward psychrometer) and three independent variables; shortwave radiation, wind velocity and wind direction; in various combinations. Ten minute average values were calculated from the one minute recorded values and an analysis was undertaken as follows.

From a linear model using a regression of ΔT_S on all three available variables, fitted as :

$$\Delta T_S = \alpha + \beta DD + \gamma VV + \varepsilon RS$$

(where: ΔT_S = dry starboard temperature - dry forward temperature, DD = wind direction, VV = wind velocity on the forward mast, RS = short wave solar radiation on the starboard sensor, α, β, γ ,ε = constants)

It was found that RS is the most significant variable in the model (see Appendix I). The exclusion of RS causes the correlation of the model to fall rapidly.

From the analysis the best fit model was found to be:

$$\Delta T_S = \alpha + \gamma VV + \varepsilon RS + \phi(VV*RS) \qquad \text{(model 1)}$$

(where: α = 0.0018, β = 0.00489, ε = 0.00178, ϕ = -0.000175)

The correlation coefficient of the model is too small for it to be used for prediction. This model explains 36.6% of the variance (compared to 17.6% explained by the mathematical model), of which 1.8% is explained by γVV, 5.1% by α, 7.8% by $\phi(VV*RS)$, and 21.9% by εRS.

Only about 40% (square of the correlation coefficient) of the original observed data was explained by a linear regression model containing shortwave radiation and wind speed (model 1). But the smoothed envelope data (data with diurnal variation removed) gave a better correlation than the original data, as the short period variance (noisy data) had been smoothed out (see Appendix I).

4.4.4 Effective Lag Coefficient of Psychrometer

It can be noted that the product of wind speed and solar radiation were prominent in both the statistical and mathematical models.

From the statistical analysis, model (1) can be written

$$\Delta T = \varepsilon RS + \phi(VV*RS) + \text{other terms} \qquad \text{(model 1)}$$

The temperature difference between the two psychrometers calculated from the energy balance equation is:

$$\Delta T = \lambda A RS / C \quad (6)$$

where: C is the heat capacity of the psychrometer, λ is the lag coefficient, RS is the incident solar radiation (W/m^2) and A is the area illuminated.

$$\text{let } \lambda = \lambda_o + \text{function(VV)} \quad (7)$$

From (6) and (7)

$$\Delta T = \lambda_o A RS /C + \text{function(VV)} A RS /C \quad (8)$$

comparing (model 1), (7) and (8)

$$\lambda = C(\varepsilon + \phi) / A \quad (9)$$

where the dimensions of ε and ϕ are dimensionally in terms of RS,..A and VV (where VV is measured in m/s, RS is measured in W/m^2, and A is .measured in m^2).

Now: C = heat capacity = specific heat capacity * mass

Specific heat capacity of psychrometer (steel) = $0.48*10^3$ J/Kg/°C, Mass of empty psychrometer = 0.87 Kg, Mass of psychrometer full of water = 1.48 Kg

Therefore: C = 417.6 J/Kg/°C when psychrometer is empty

and C = $0.87*0.48*10^3 + 0.61*1*10^3$ = 1028 J/Kg/°C when psychrometer is full

Area of psychrometer = 0.01 m^2, ε = 0.00178, ϕ = -0.000175

Substitution in (9) gives:

λ = 67 seconds when psychrometer is empty, λ = 165 seconds when psychrometer is full

This assumes the psychrometer is made from steel, whereas it is actually made from die-cast metal. The difference in specific heat capacities would not greatly effect the time lag (λ). Therefore the effective time lag of the heating up of the psychrometer due to shortwave radiation for all wind speeds is in the order of a few minutes.

5. ANEMOMETER ERRORS

The pre and post-cruise wind speed values linearly increased as frequency increased. Regressing pre and post-cruise values for increasing frequencies resulted in the linear regression equation:

$$P_2 = -0.135656 + 0.96173P_1$$

where: P_1 = pre-cruise values, P_2 = post-cruise values

Thus the original pre-cruise calibrated data for the wind speed from the main mast anemometer may need to be re-calibrated. Figure 16 shows there are no obvious step changes in the difference between the main mast and foremast anemometer readings during the cruise, which suggests that the main mast post-cruise calibrations are valid.

Figure 17 shows the relative mean wind speed of the main mast anemometer after post-cruise calibrations. In order to compare these readings with those from the forward mast it is necessary to allow for the change in the mean wind speed with height, since the

anemometer on the main mast is higher than the forward mast (23.8 metres and 15.1 metres respectively).

Using CD 47 data and assuming neutral conditions (ie. a logarithmic wind profile)

$$M/u_* = (1/k) \ln (z/z_o) \quad (10)$$

where: M = mean wind speed, u_* = friction velocity, k = 0.4, z = height, z_o = aerodynamic roughness length $\approx 10^{-3}$. Since u_* is the same at each sample point, substituting values for the forward and main mast in (10) gives:

$$M_2 = M_1 (\ln(z_2/z_o)/\ln(z_1/z_o)) \quad (11)$$

substituting relevant anemometer heights in (11) then gives:

$$M_2 = 1.062\, M_1 \quad (12)$$

Therefore the height difference between the two anemometers would cause about a 6% difference in wind speeds.

Figure 18 shows the actual difference between wind speed readings from the main and foremast anemometers as a function of wind speed; after post-cruise calibrations have been applied, and the affects of the height difference between the two anemometers have been removed. Figures 17 and 18 show that when the wind is on the port bow (between 270° and 30°), the main mast anemometer reads 4% higher than the foremast anemometer, probably due to the acceleration of the air flow over the ship. Between 90° and 130° the main mast anemometer reads higher than the foremast, due to sheltering of the foremast anemometer by the foremast; and higher between 130° and 210° due to sheltering by the ship.

6. QUALITY OF RADIATION DATA

Figure 19 compares the shortwave radiation reading from the starboard sensor with that from the port sensor for CD 47. The port and starboard sensors compare well except at high solar radiation values (over 350 W/m^2), where the port sensor reads lower than the starboard sensor. This occurs mainly on two days of the cruise, day numbers: 164, 167 (Figure 21, 22). When these two days are removed, the port and starboard radiation sensors compare well (Figure 20). The cause of the sensor difference is unknown, but reasons suggested in discussion included temporary failure of the temperature compensation circuit or a sticking gimbal mount.

7. SUMMARY

There was an error in the readings from the forward dry bulb temperature which read 0.45° high. The calibration certificates for the psychrometers (showing pre-cruise and post-cruise figures), show no significant changes in calibration for the period of deployment. Therefore the discrepancy of dry bulb temperatures on the foremast can not be accounted for by means of shift in the calibration. It is possible that the frequency signal may have been miscounted at the logger, resulting in a lower value of temperature being

recorded. Funnel heat also caused spurious psychrometer readings; the temperature difference between the forward and starboard psychrometers increases when the relative wind direction was between 200° and 250°. This effect is not clearly seen for the temperature difference between the forward and port psychrometers. The reason for this is not known.

From a statistical analysis using starboard sensor data for CD 47, it was found that the differences between temperature readings from the psychrometer on the forward mast and those on the wheelhouse top tended to be directly affected by shortwave radiation, with a modification to take into account the relative wind. Port sensor data for CD 47 showed the same results.

After post-cruise calibrations have been applied to the main mast anemometer, and the effects of the height difference between the two have been removed, the main mast anemometer reads higher than the forward mast anemometer by about 0.3m/s, thus implying there is speeding up over the ship.

There is no significant difference between readings from the port and starboard shortwave radiation sensors.

8. RECOMMENDATIONS

From the meteorological data for the BOFS experiment from the *RRS Charles Darwin* cruises CD 46 and CD 47; the sensor recommendations in order to calculate surface fluxes of heat and momentum would be:

Variable	Recommended sensor
Dry bulb temperature	foremast psychrometer (with 0.45°C correction)
Wet bulb temperature	foremast psychrometer
Wind speed	foremast anemometer
Wind direction	main mast wind vane
Solar radiation	maximum of port and starboard values
Long wave radiation	only one sensor available

9. REFERENCES

Birch and Pascal, 1987, A Meteorological System for Research Applications - Multimet. Pages 7-12, 5th International Conference on Electronics for Ocean Technology. Edinburgh 24th - 26th March 1987. London: Institute of Electronic and Radio Engineers. IERE publication number 72.

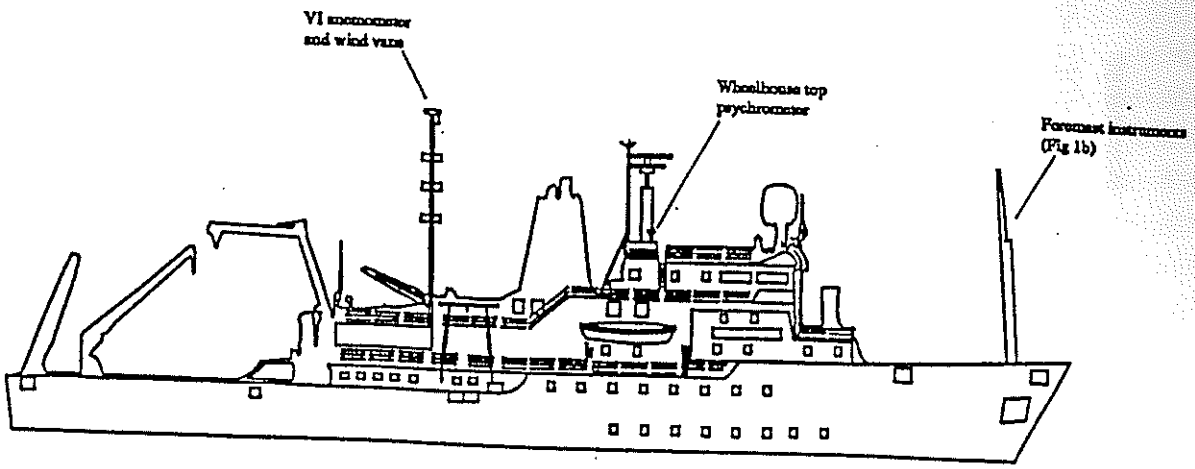

Fig 1a Position of the sensors on the *RRS Charles Darwin*

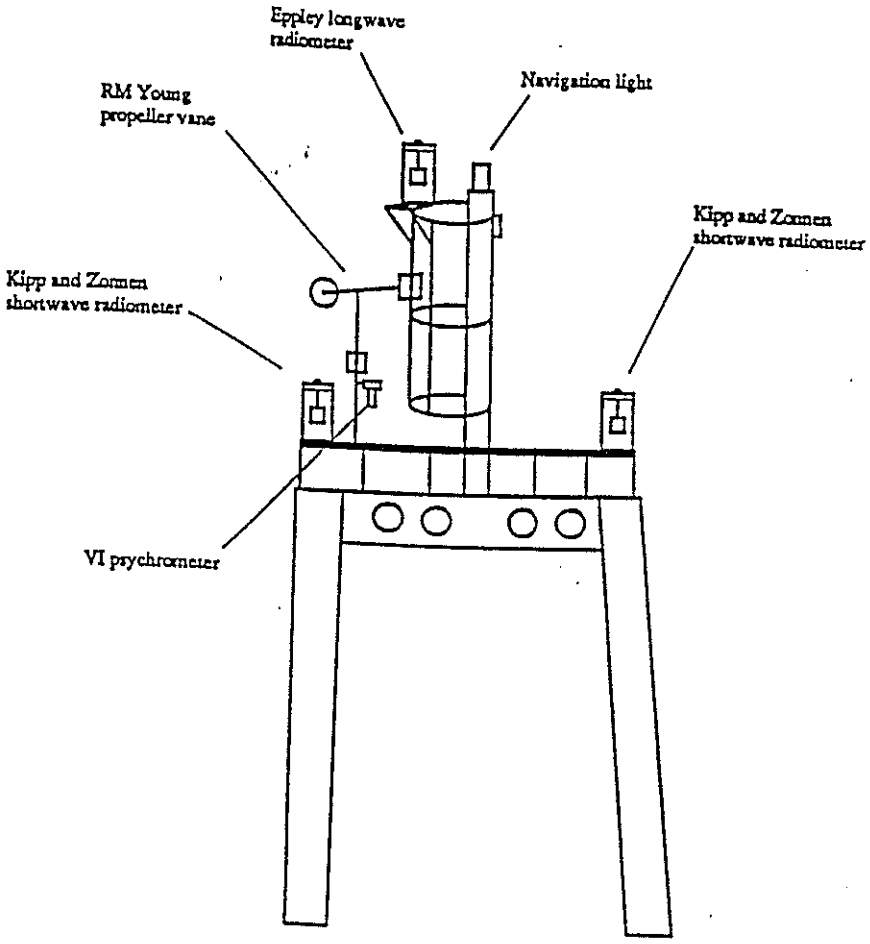

Fig 1b The Instruments used on the *RRS Charles Darwin* forward mast

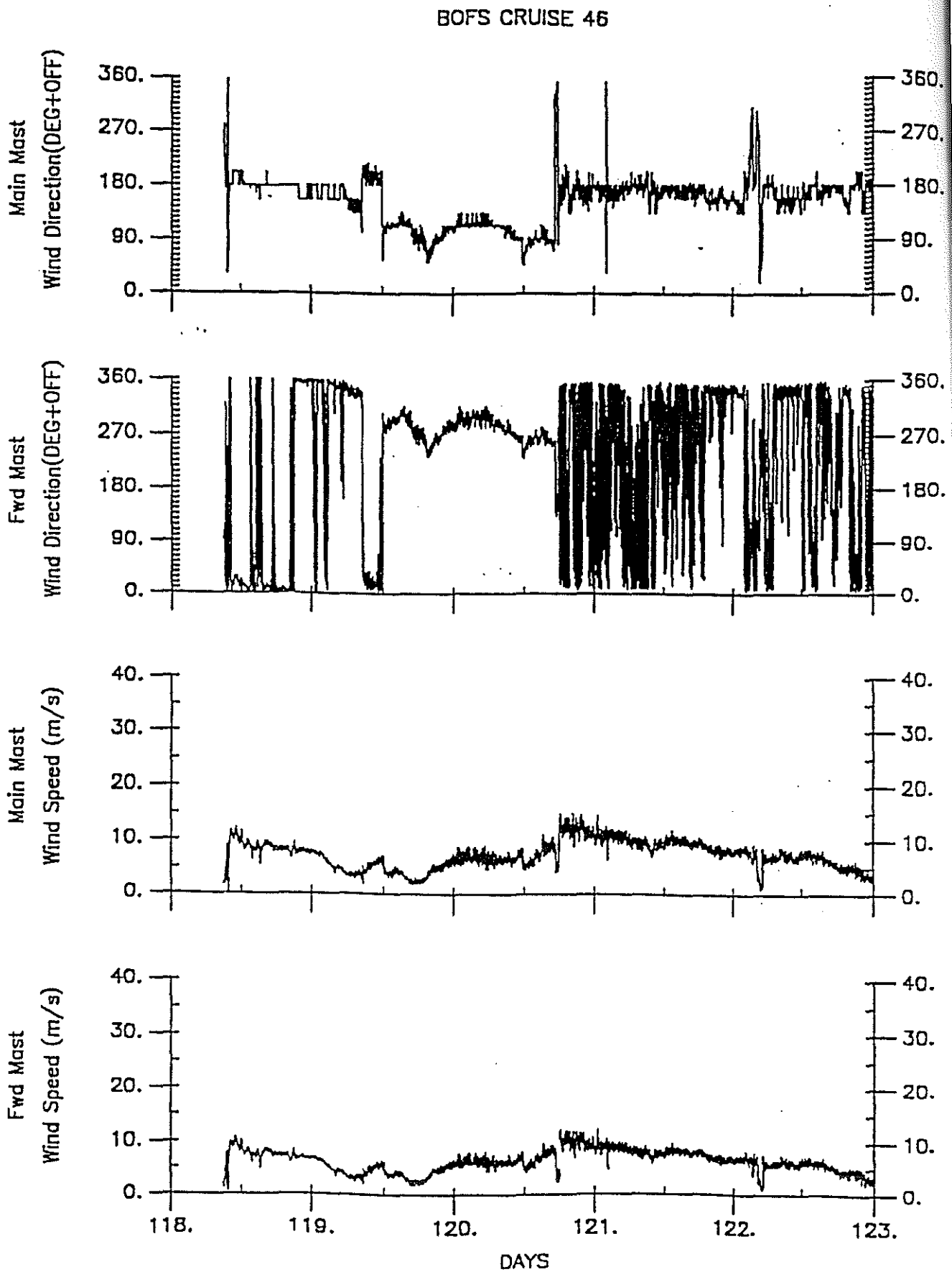

Fig 2a Time series plots showing the wind direction from the main mast and forward mast and the corresponding relative wind speeds, from day number 118 to 123.

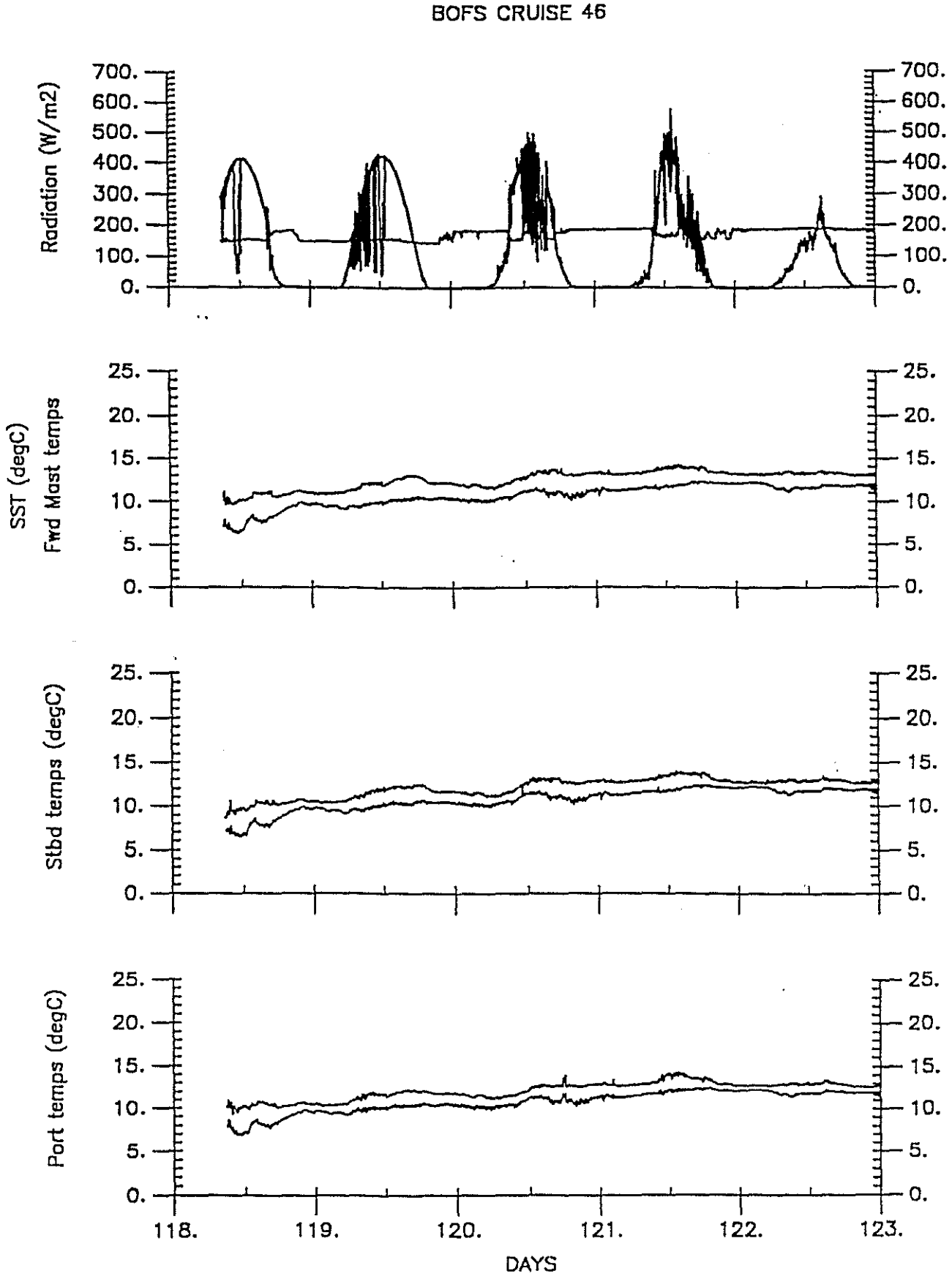

Fig 2b Time series plots showing long and shortwave radiation: wet and dry bulb forward mast temperature; and sea surface temperature where present; wet and dry bulb starboard and port temperatures; for 'despiked' data from day number 118 to 123.

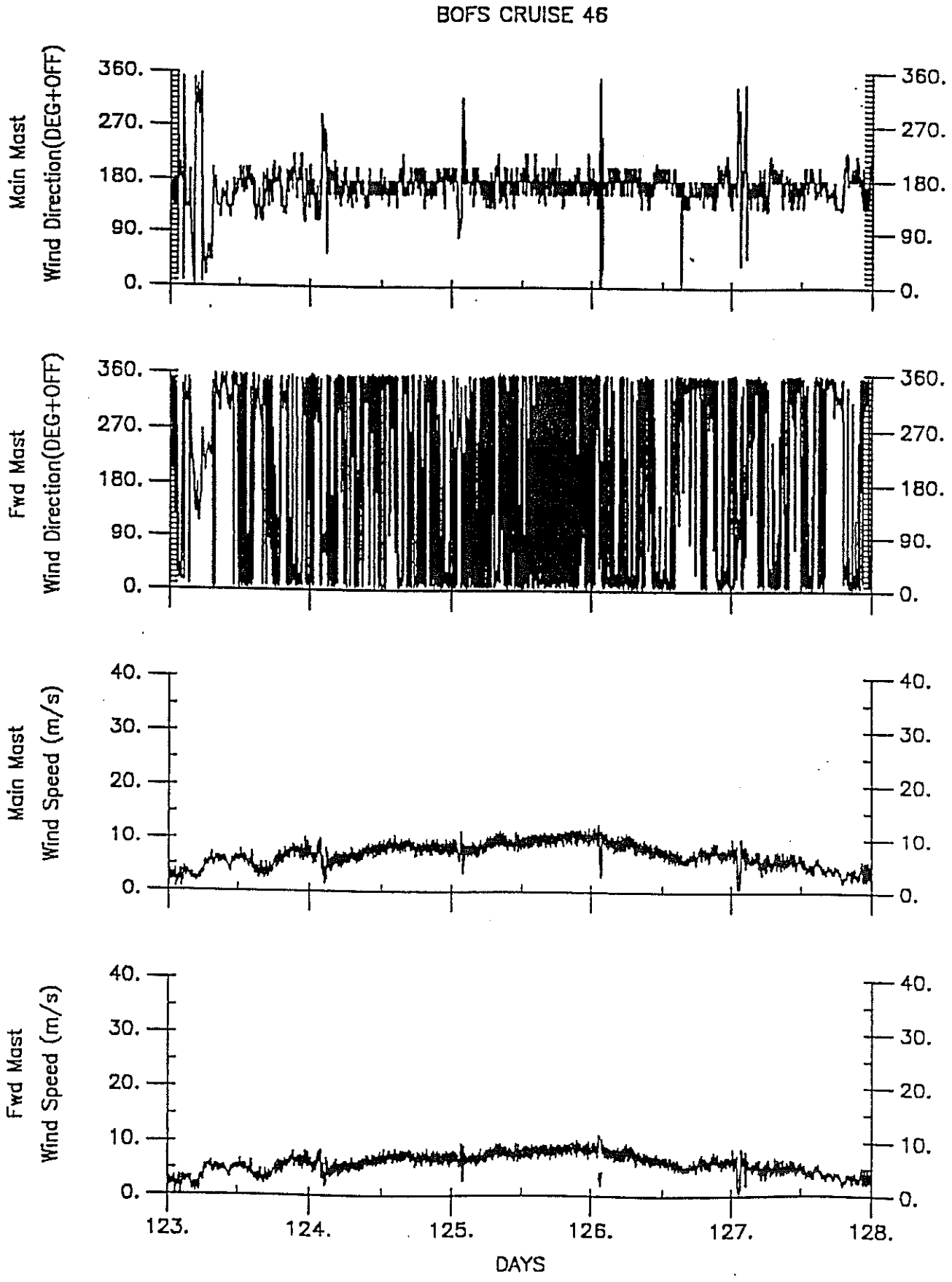

Fig 2c As Fig 2a except day number 123 to 128

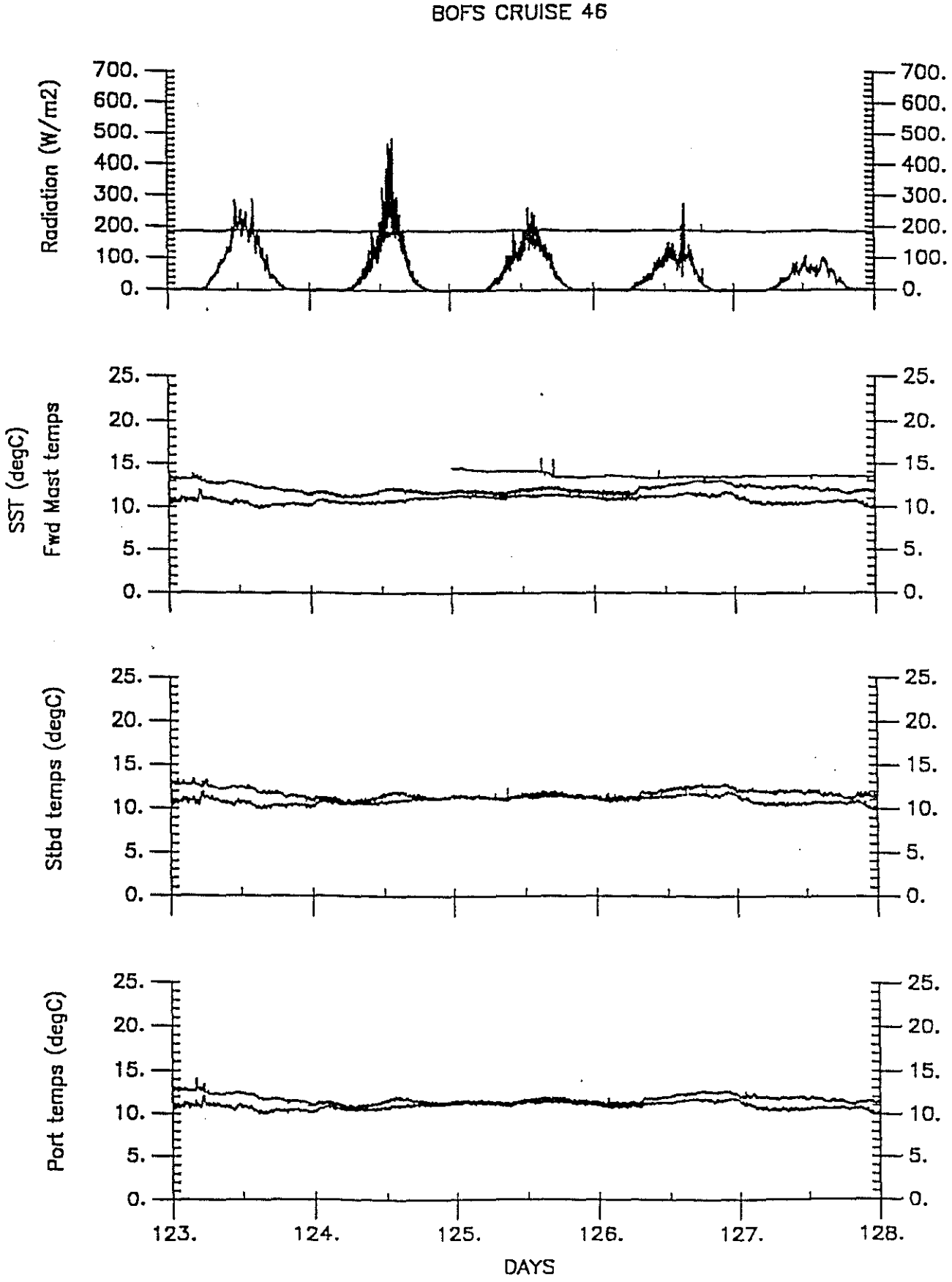

Fig 2d As Fig 2b except day number 123 to 128

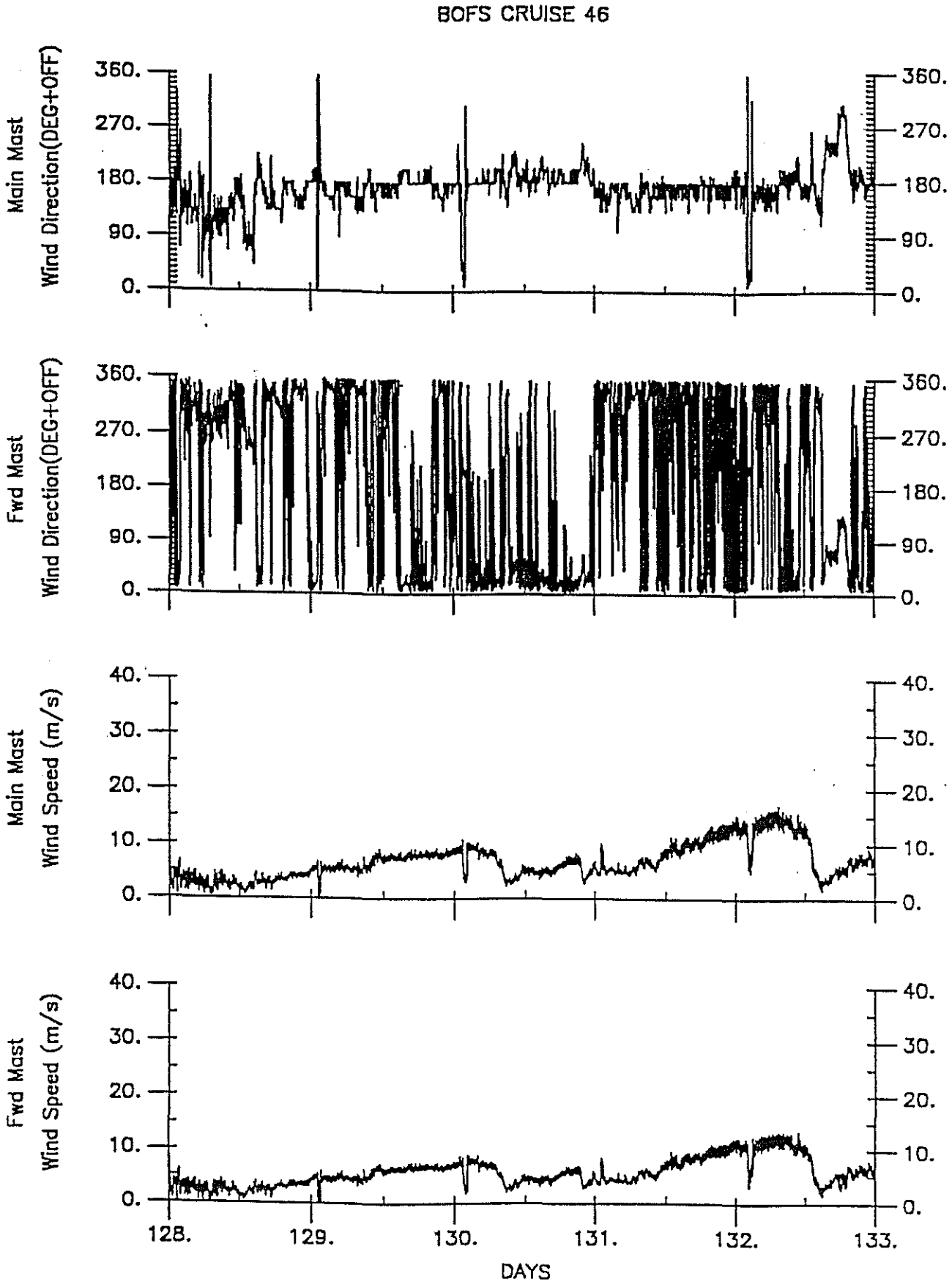

Fig 2e As Fig 2a except day number 128 to 133

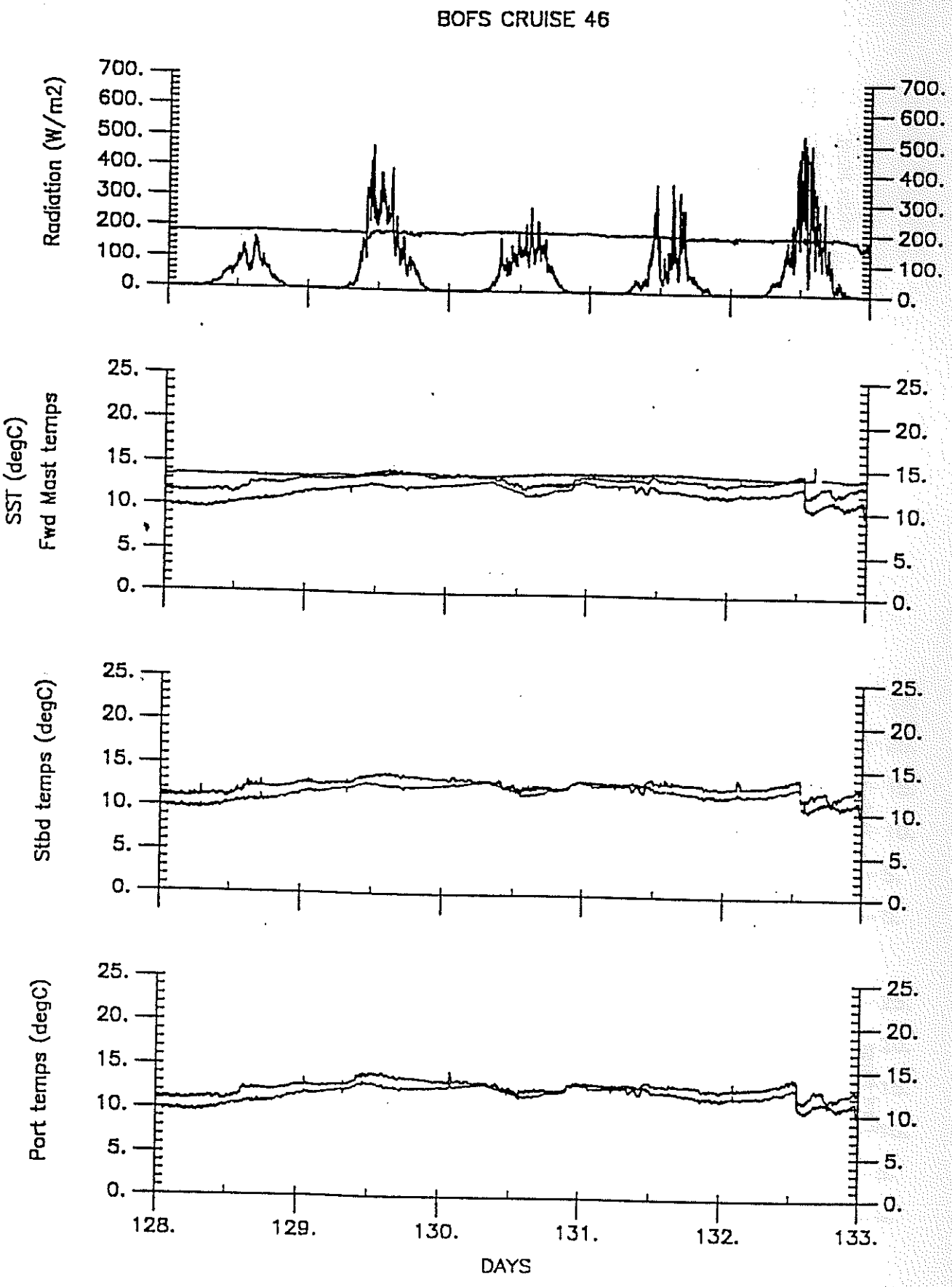

Fig 2f As Fig 2b except day number 128 to 133

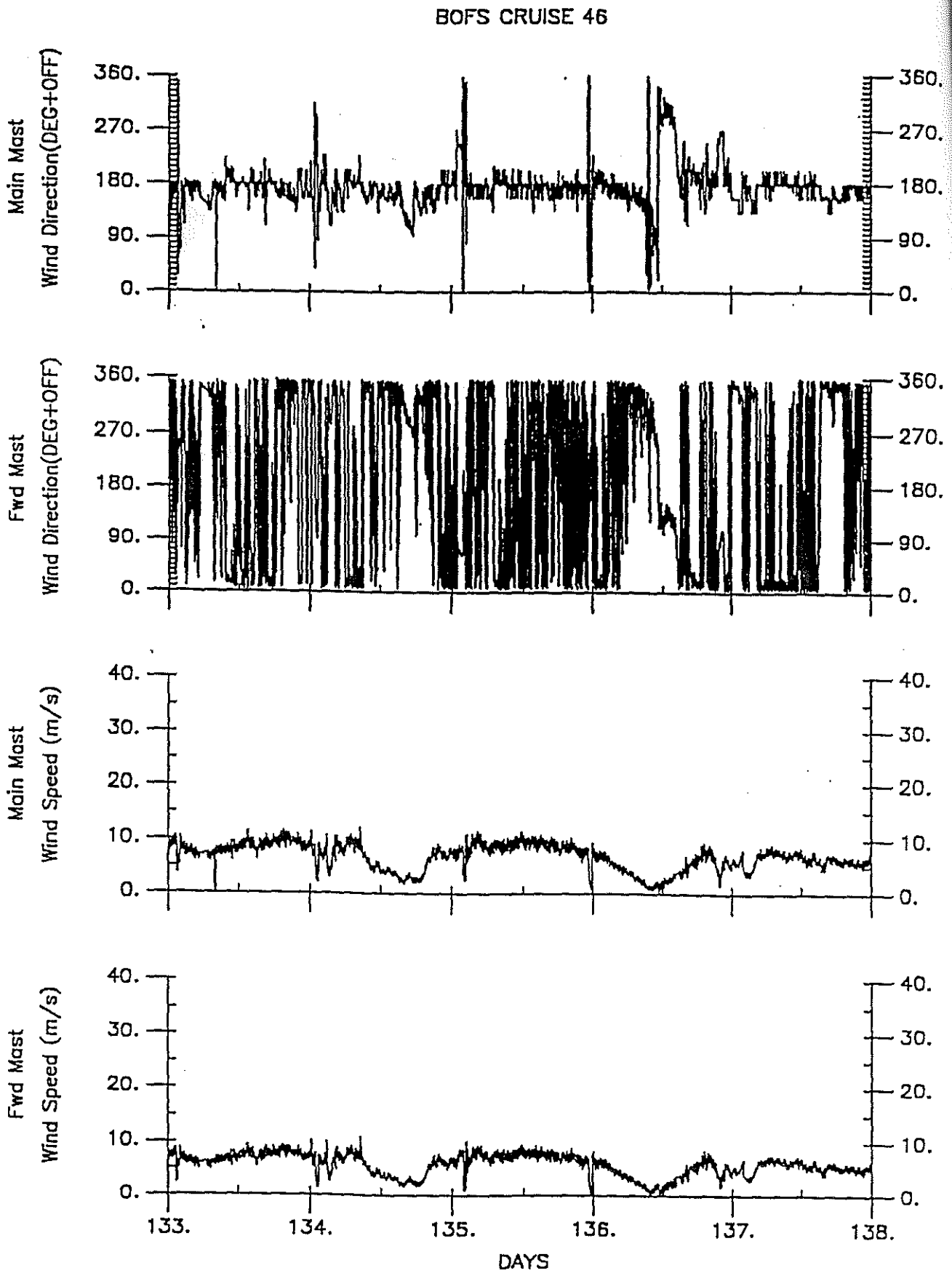

Fig 2g As Fig 2a except day number 133 to 138

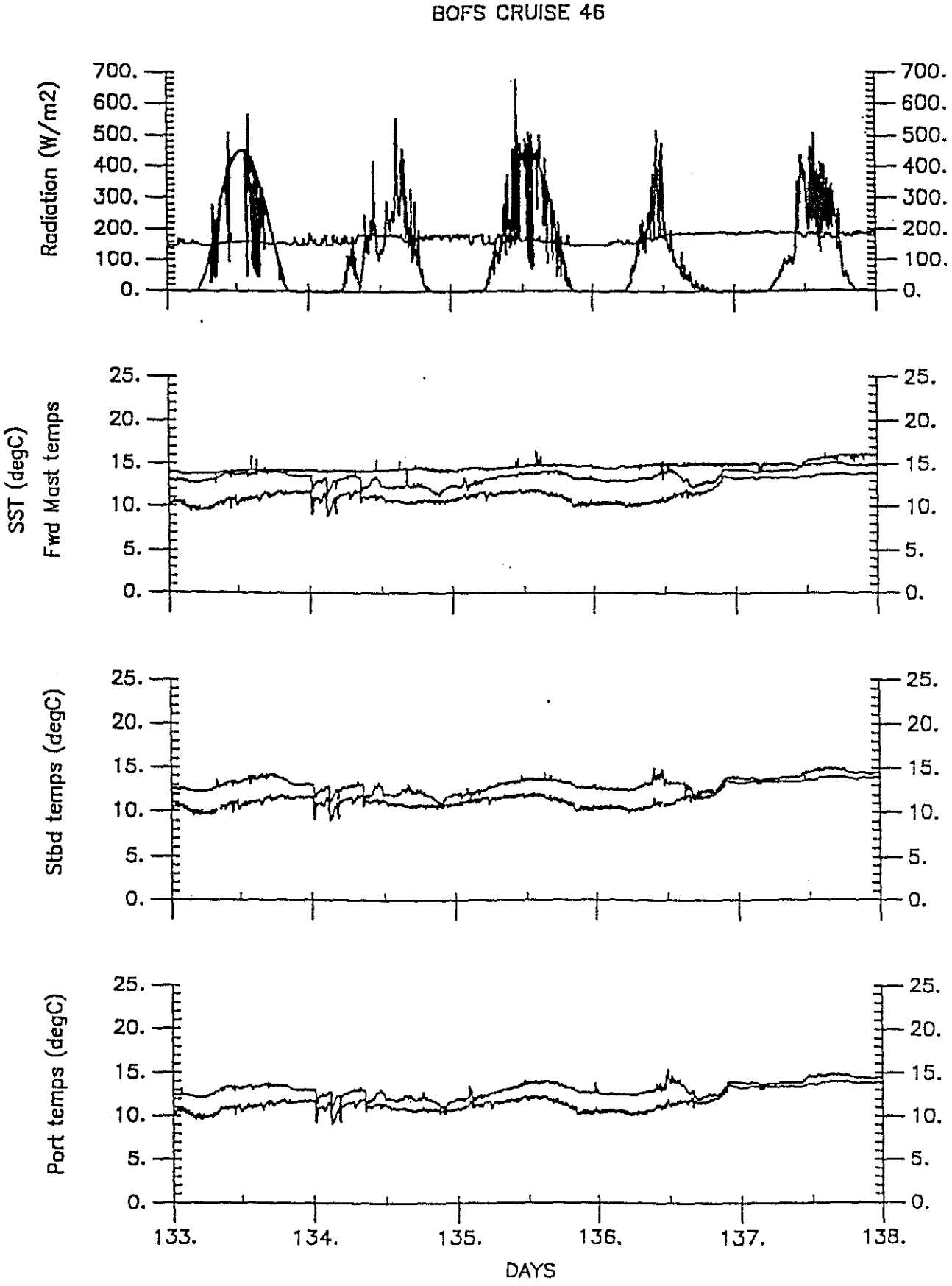

Fig 2h As Fig 2b except day number 133 to 138

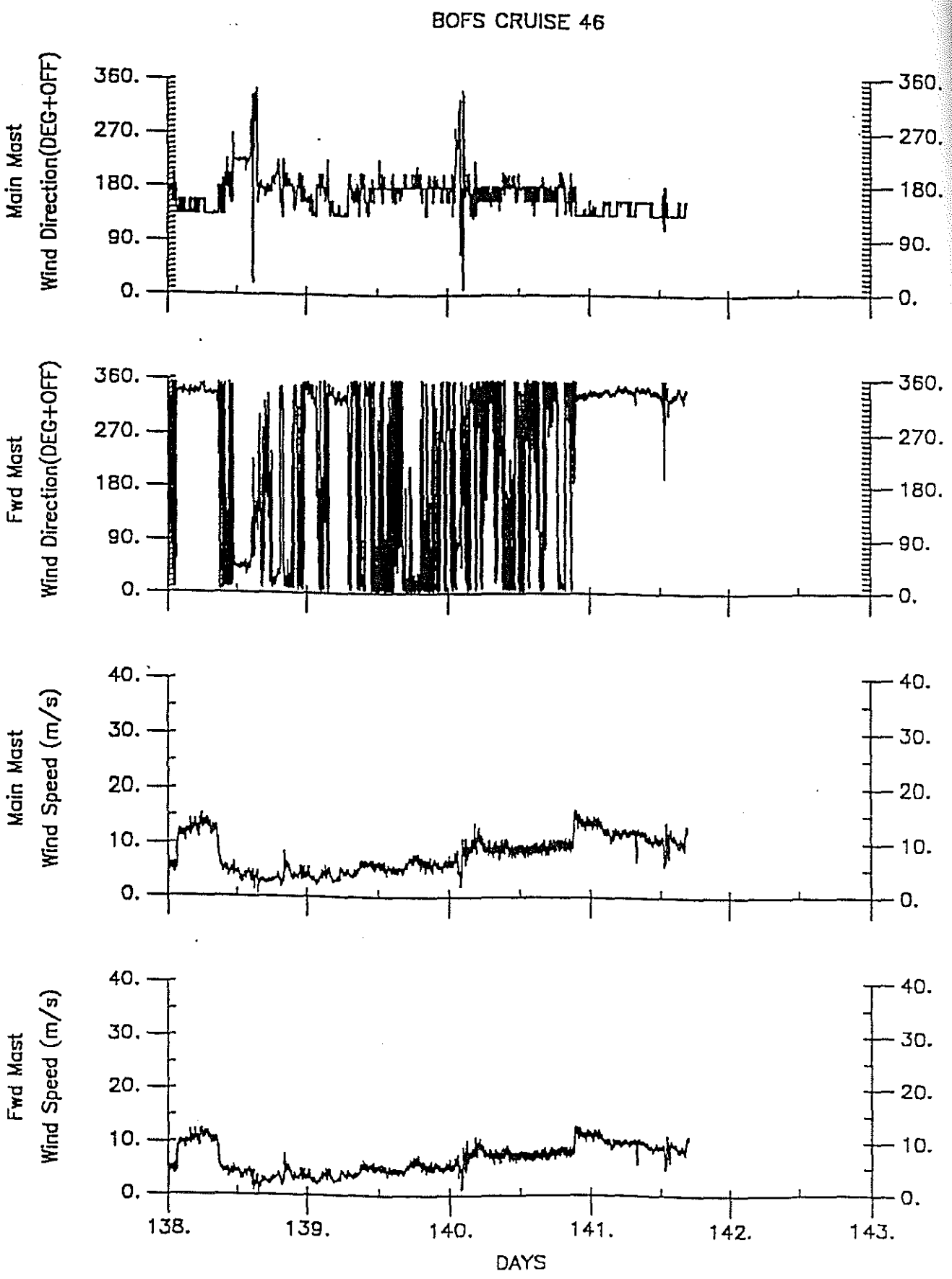

Fig 2i As Fig 2a except day number 138 to 143

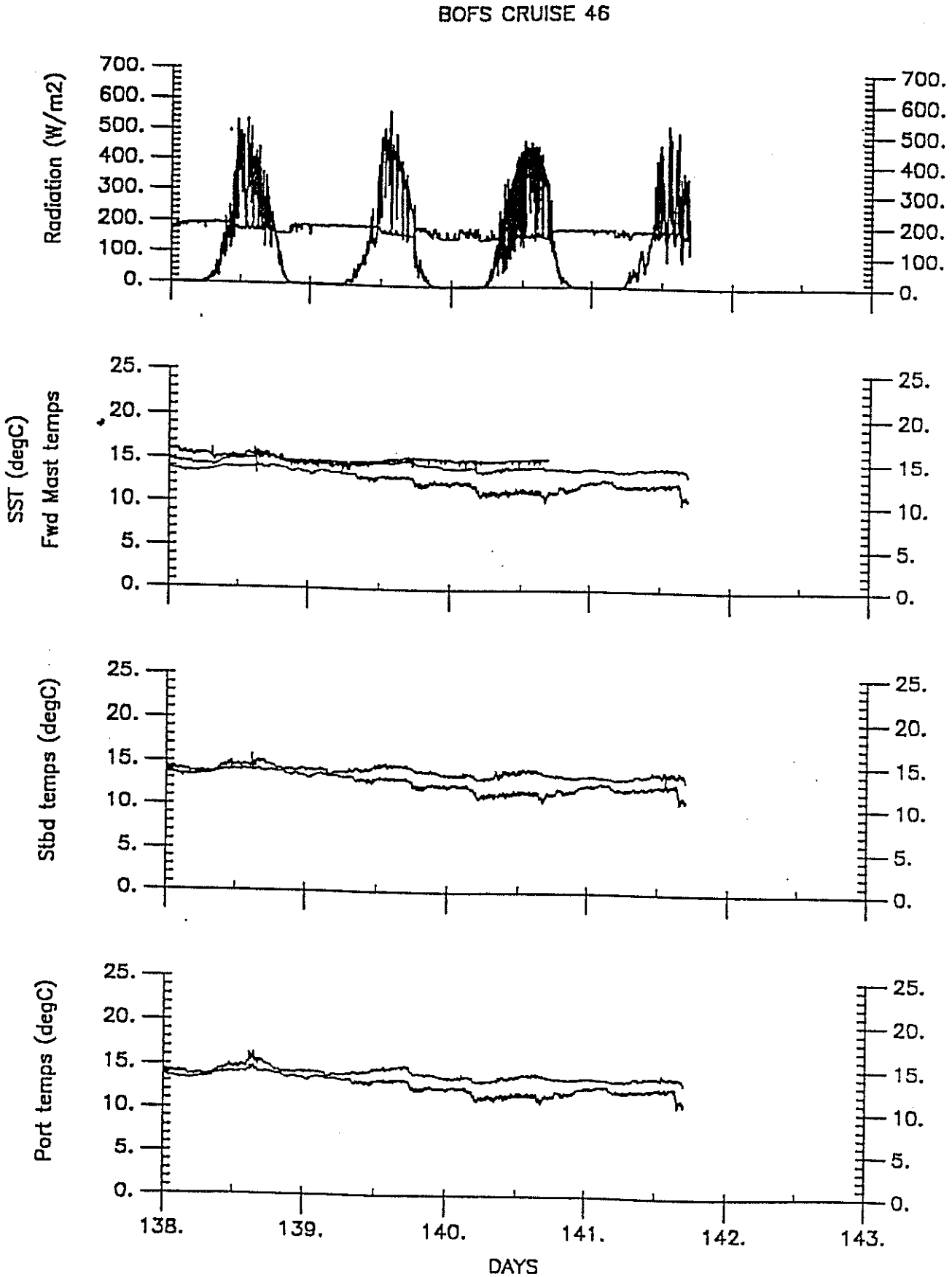

Fig 2j As Fig 2b except day number 138 to 143

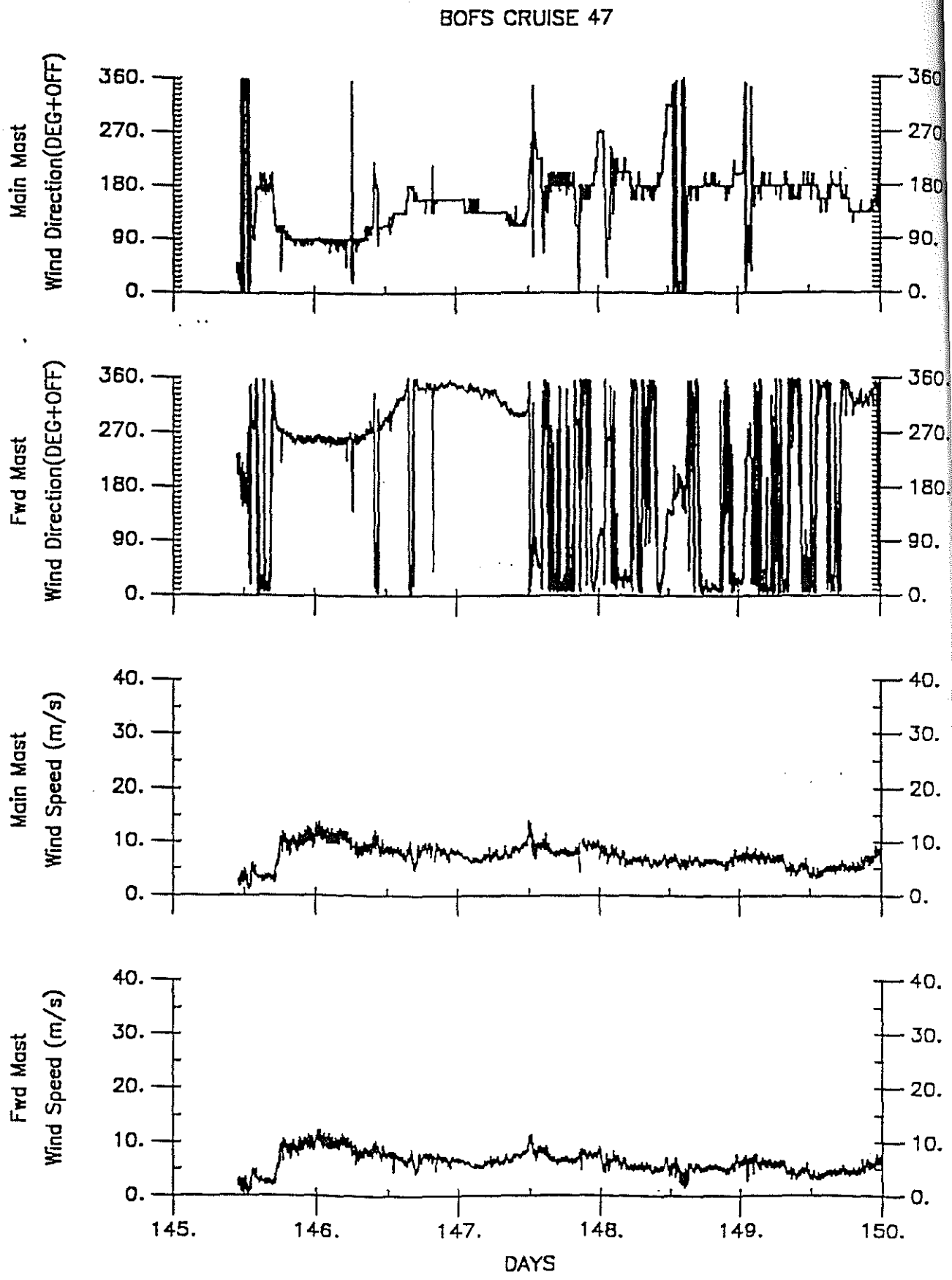

Fig 3a Time series plots showing the wind direction from the main mast and forward mast and the corresponding relative wind speeds, from day number 145 to 150.

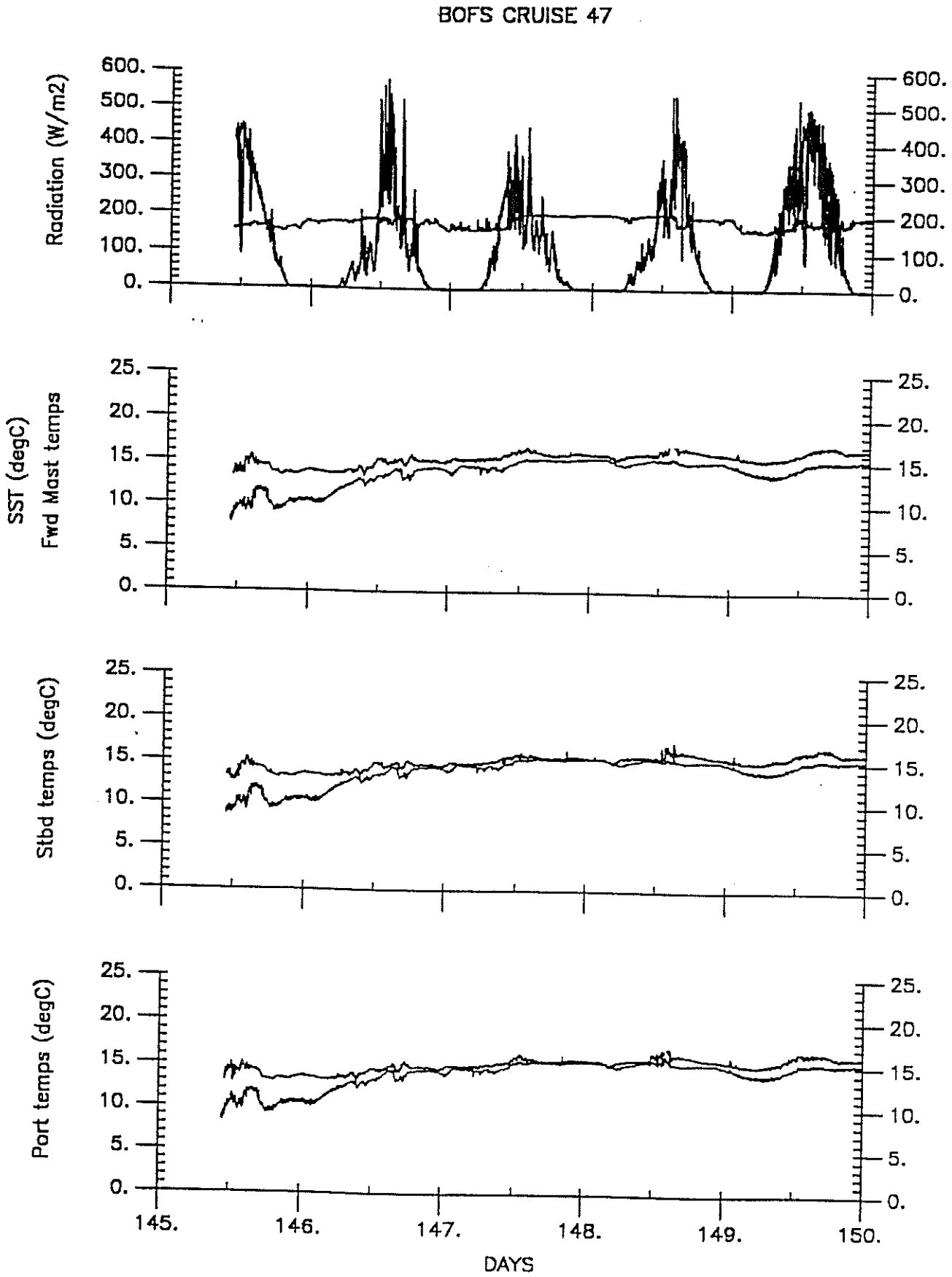

Fig 3b Time series plots showing long and shortwave radiation: wet and dry bulb forward mast temperature; and sea surface temperature where present; wet and dry bulb starboard and port temperatures; for 'despiked' data from day number 145 to 150.

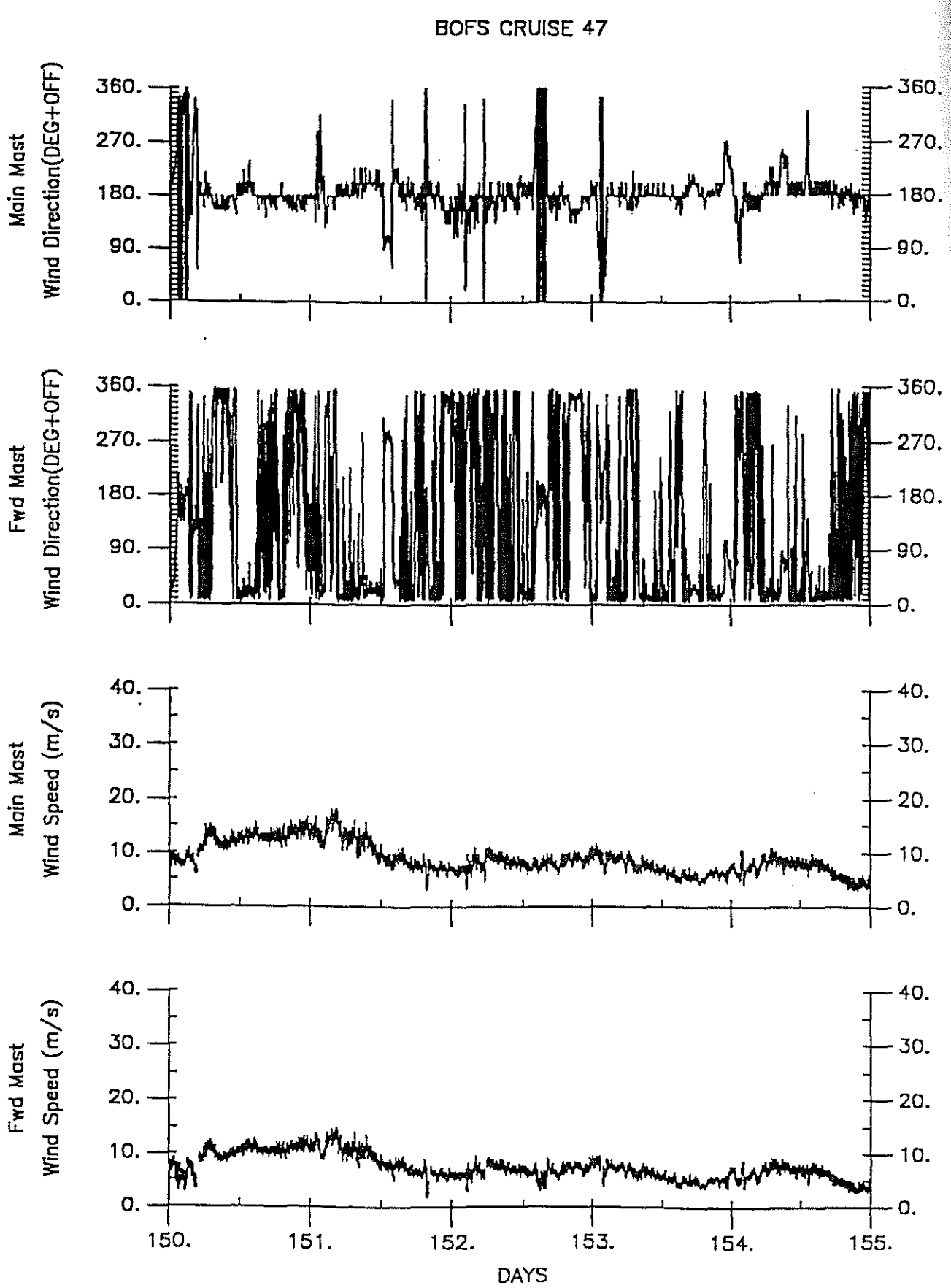

Fig 3c As fig 3a except day number 150 to 155

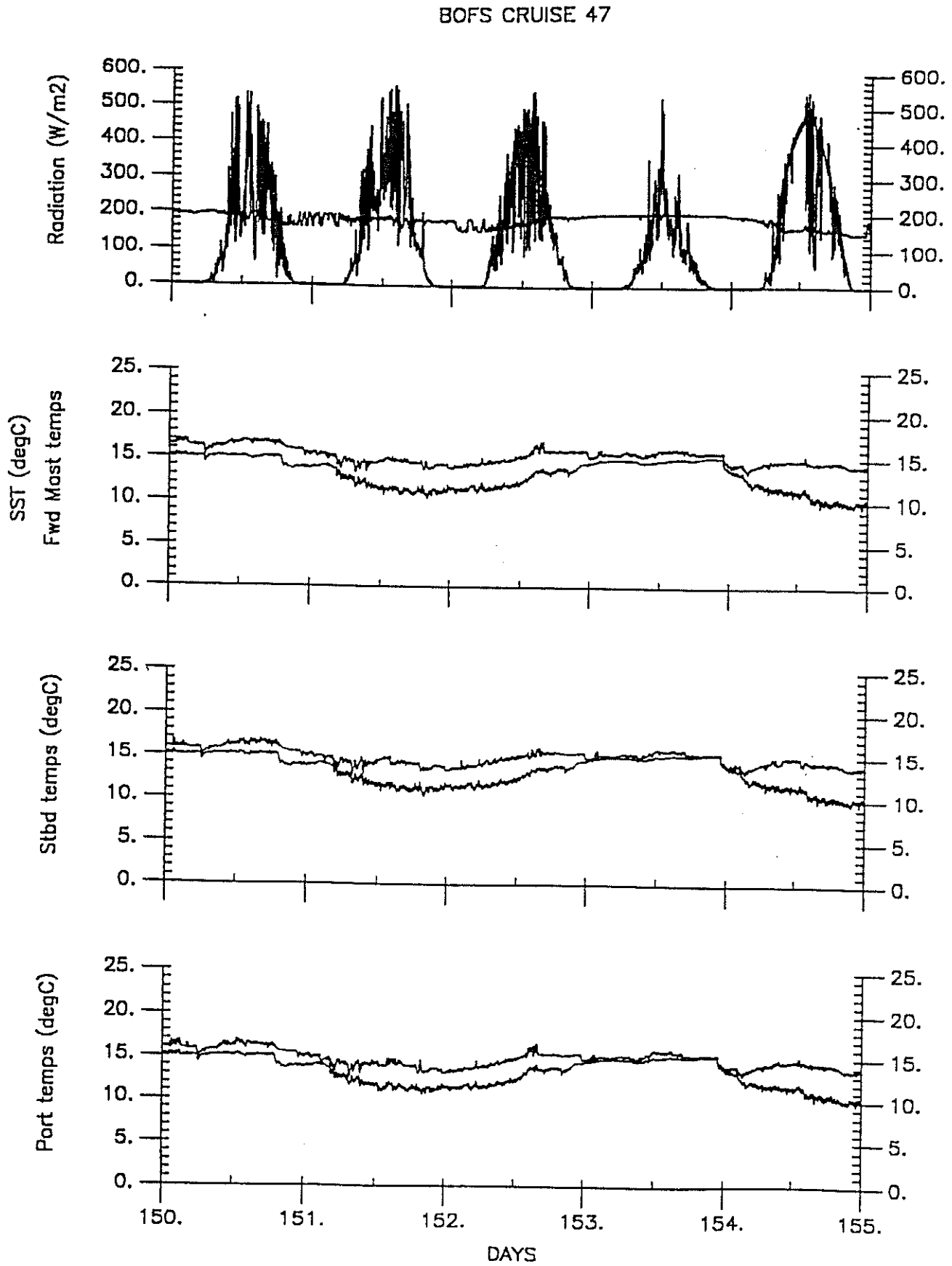

Fig 3d As fig 3b except day number 150 to 155

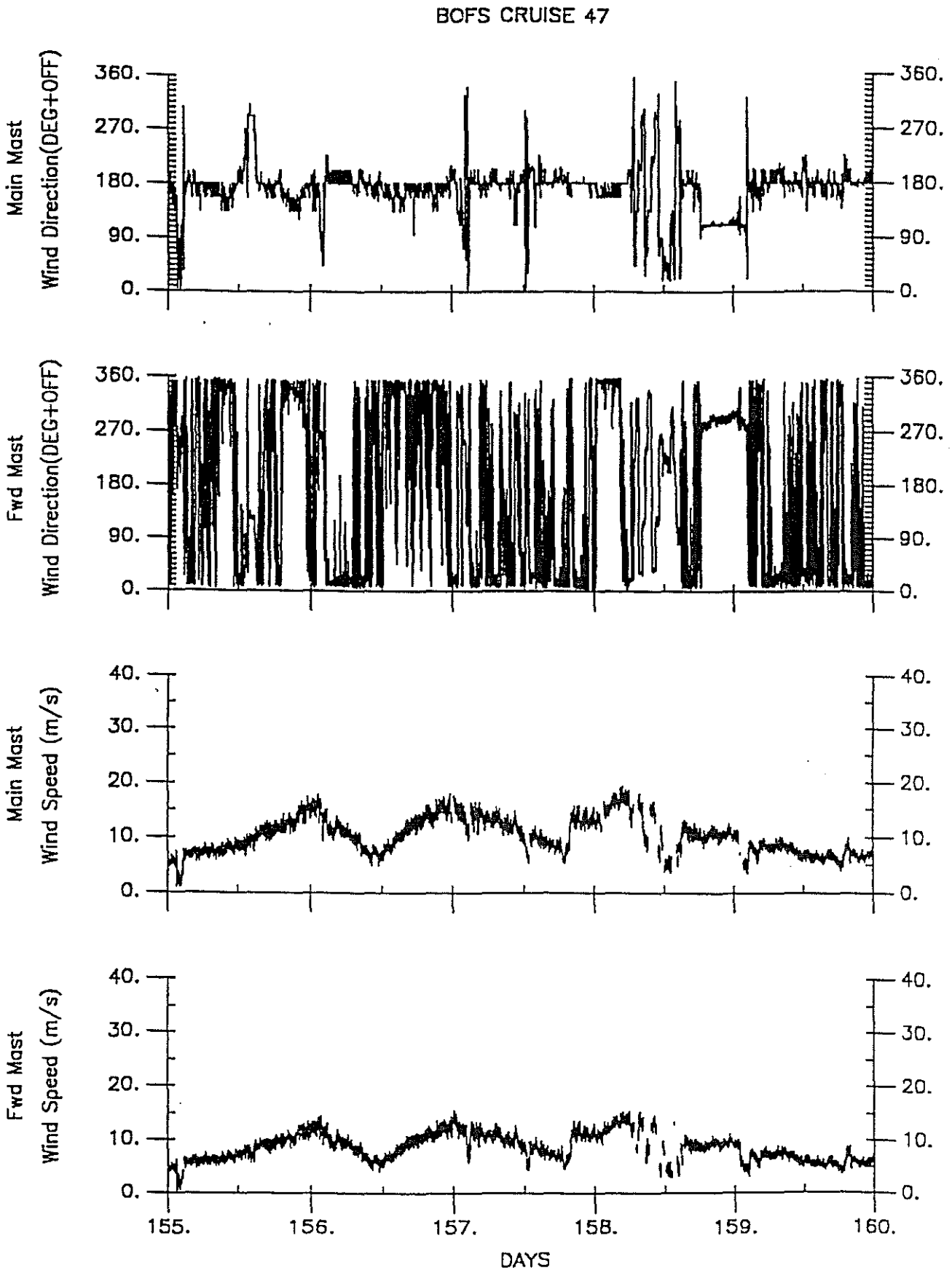

Fig 3e As fig 3a except day number 155 to 160

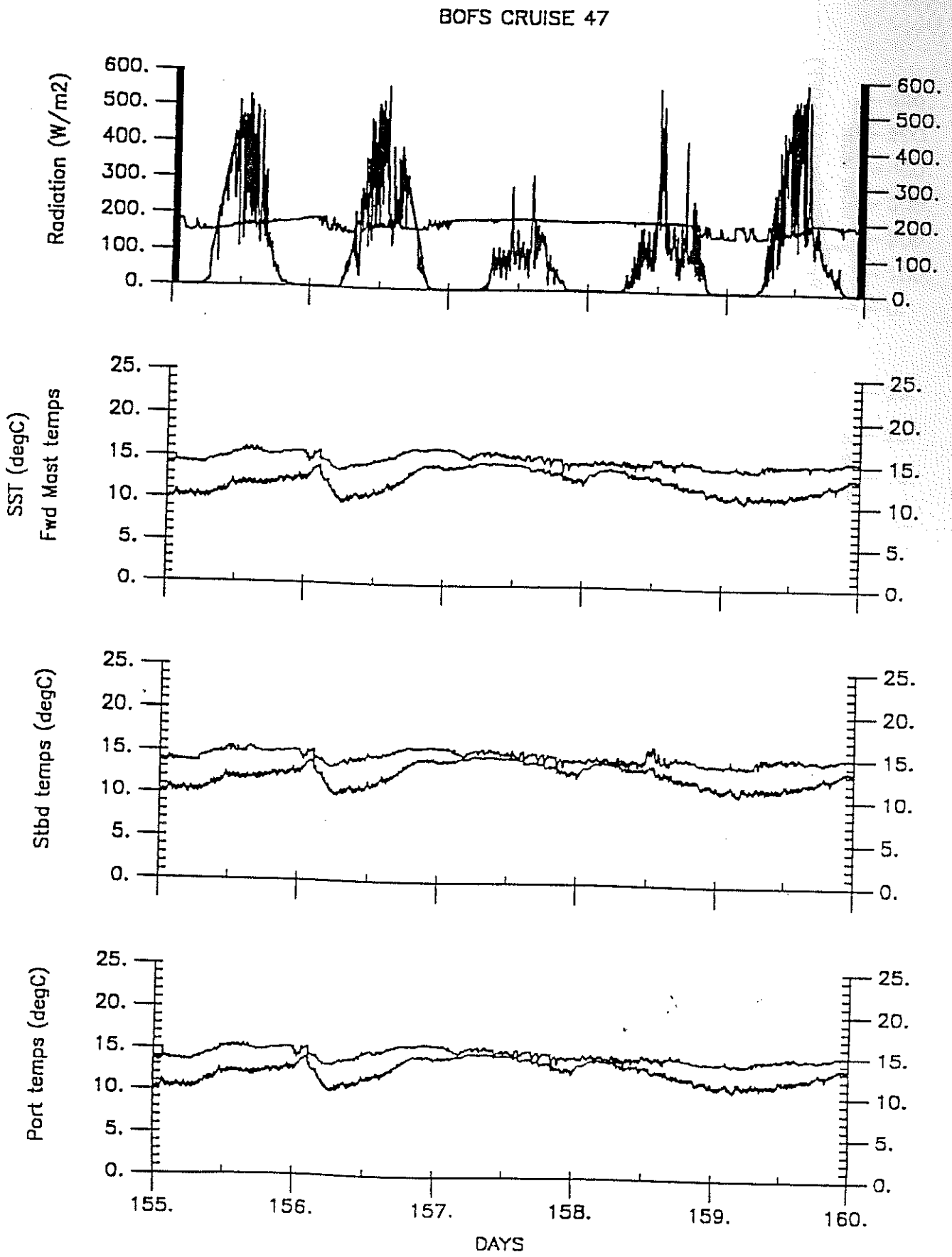

Fig 3f As fig 3b except day number 155 to 160

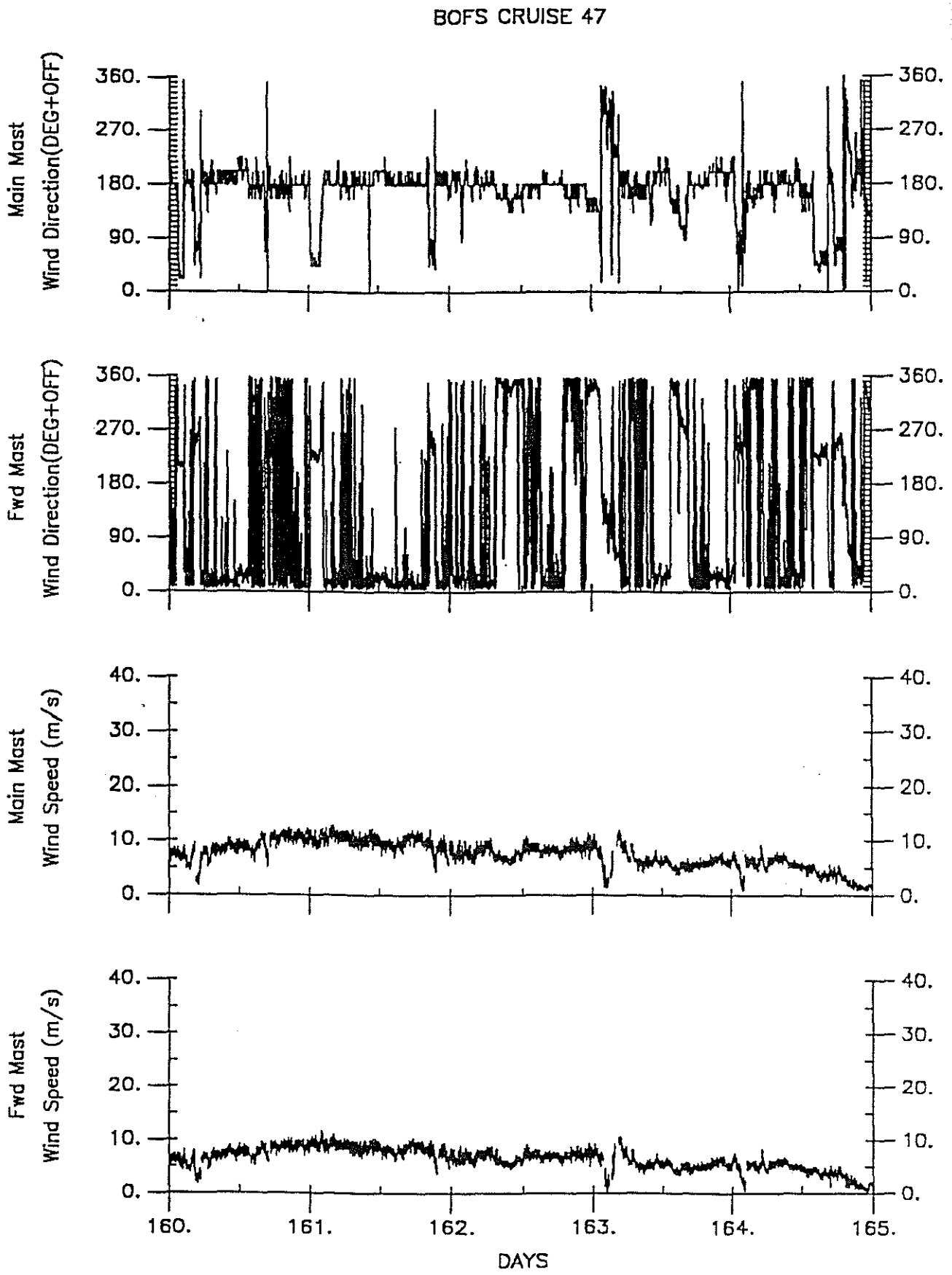

Fig 3g As fig 3a except day number 160 to 165

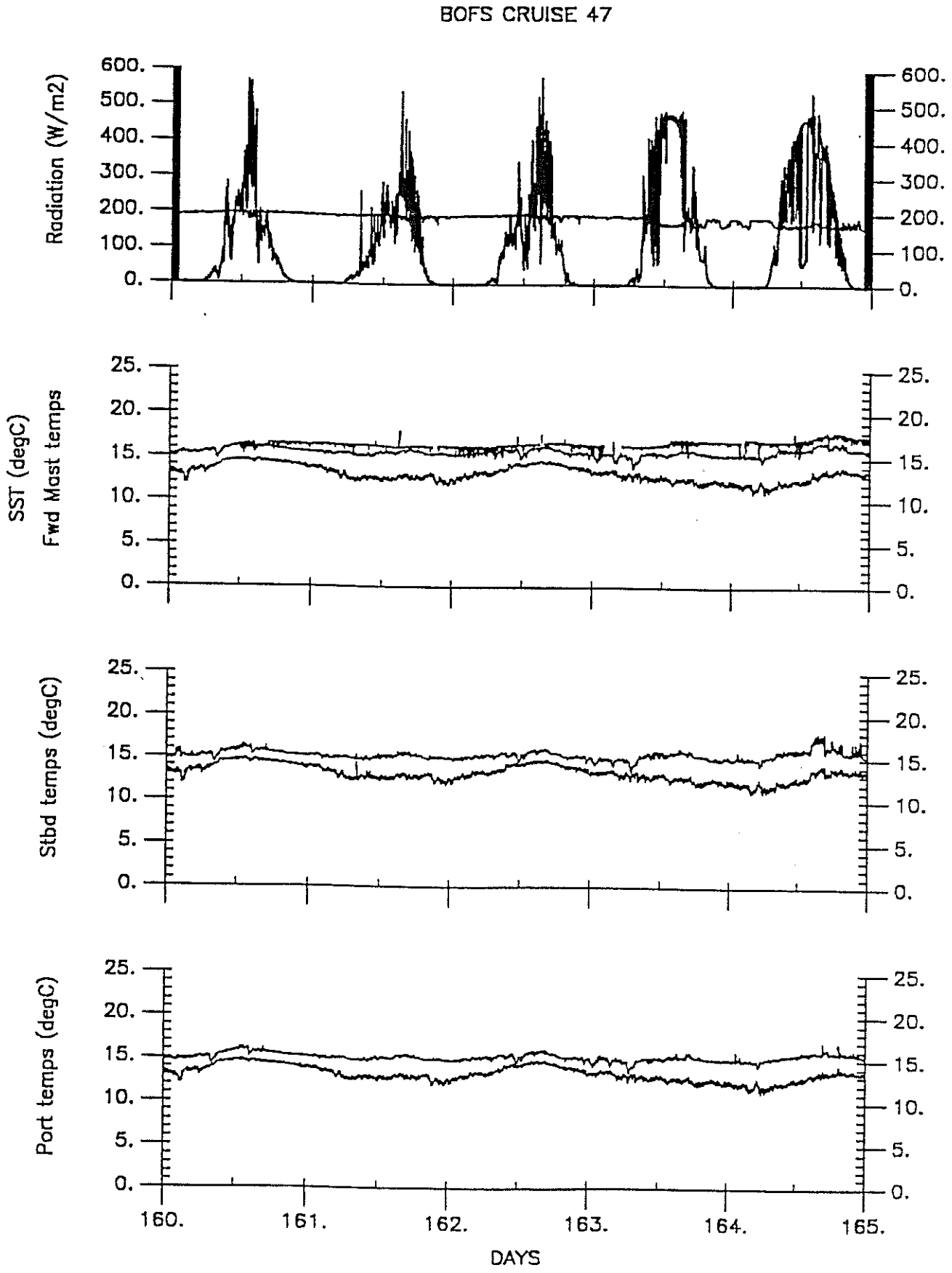

Fig 3h As fig 3b except day number 160 to 165

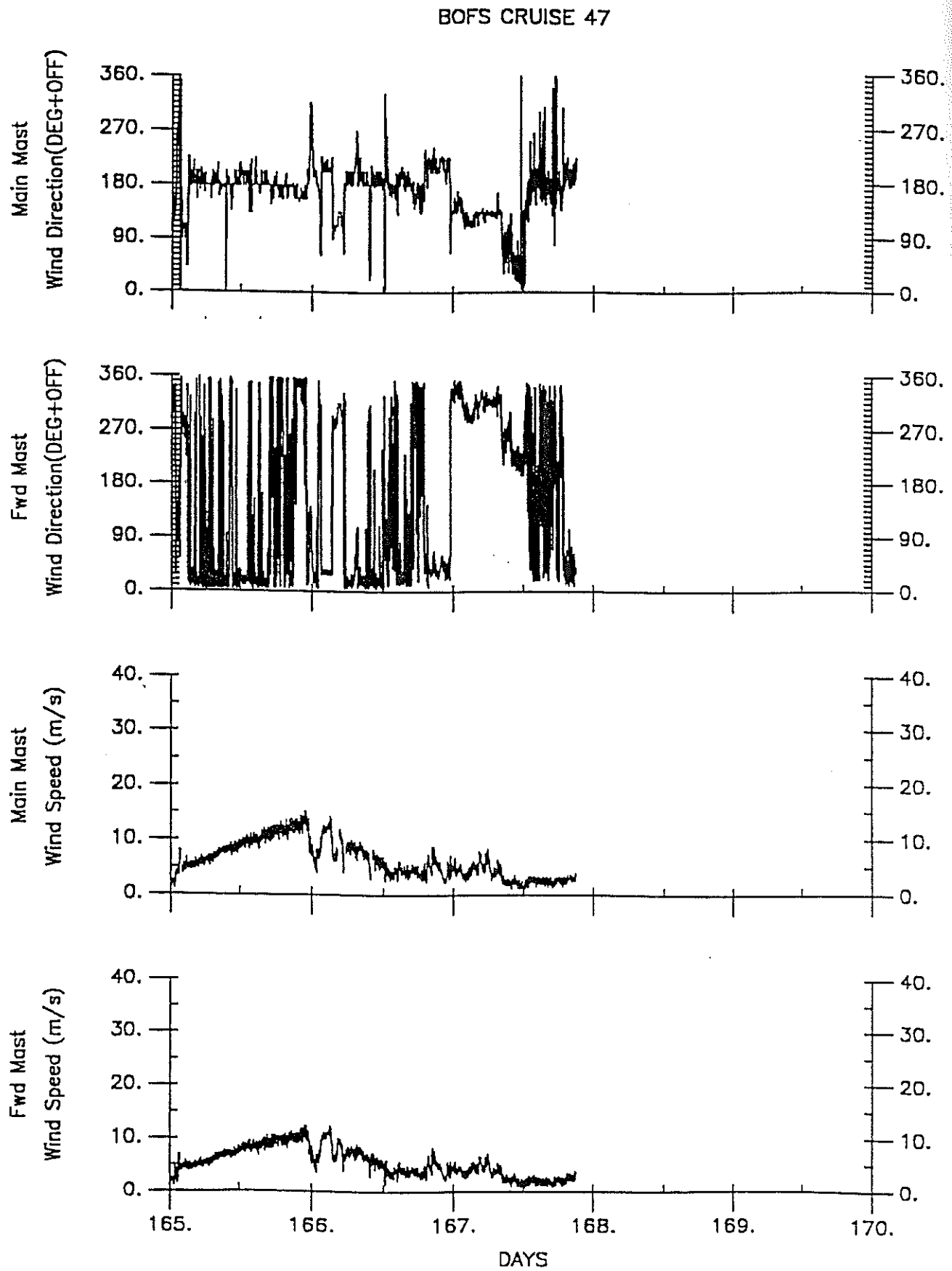

Fig 3i As fig 3a except day number 165 to 170

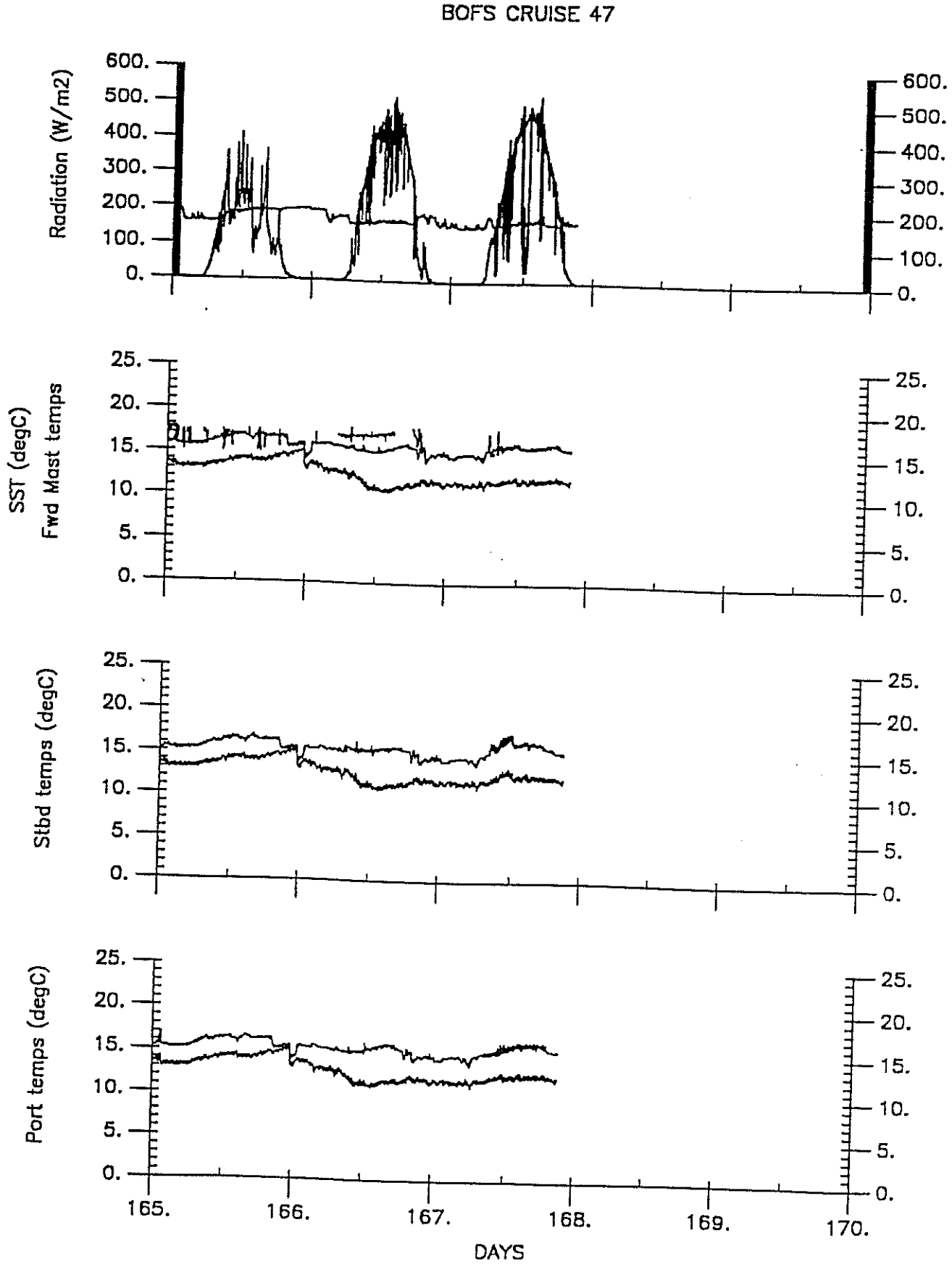

Fig 3j As fig 3b except day number 165 to 170

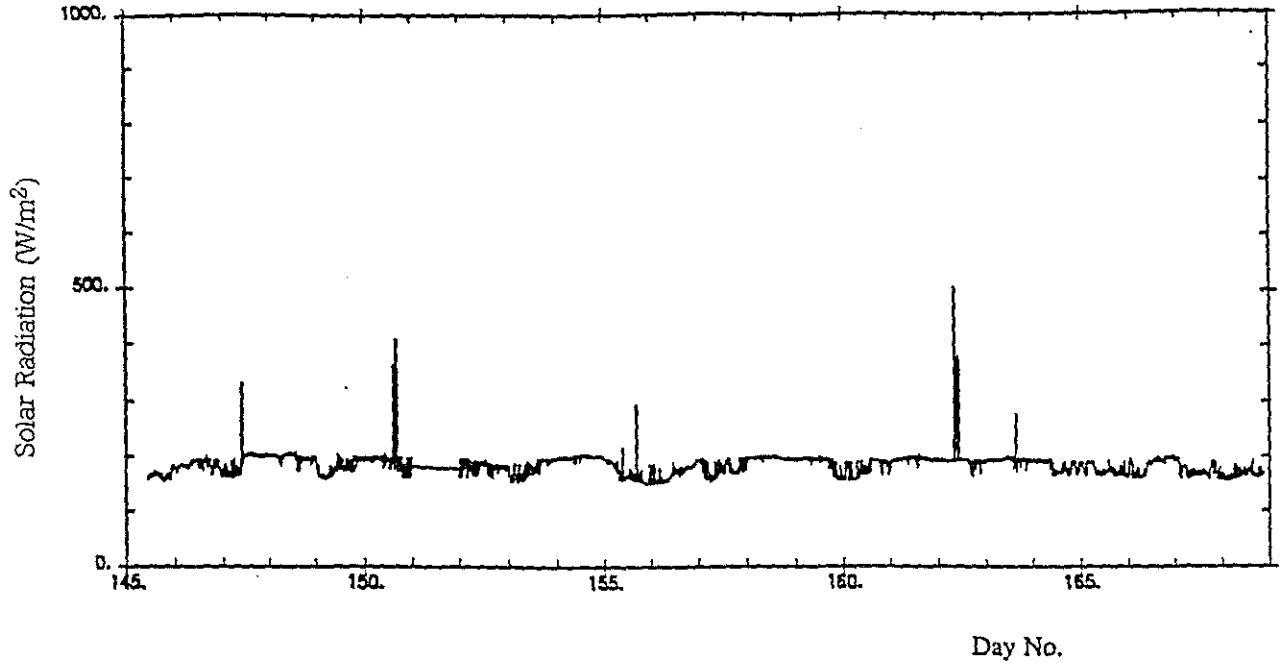

Fig 4 Original plot of long wave radiation with 'spikes'

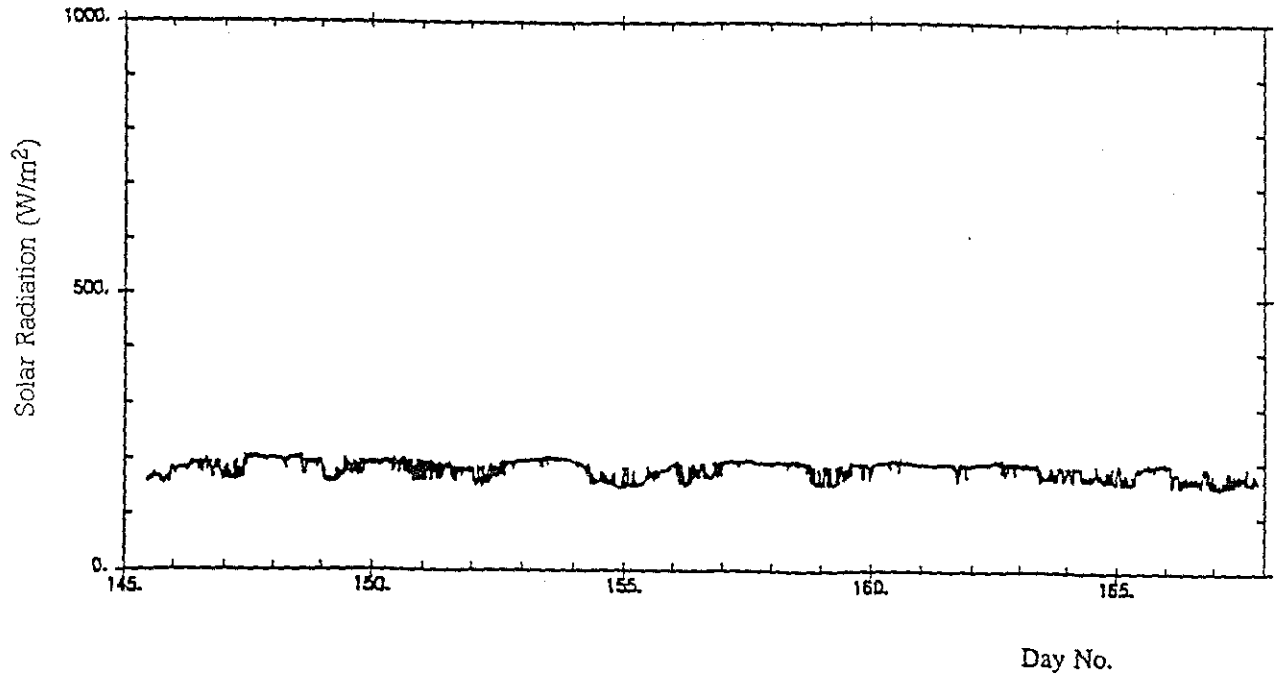

Fig 5 'Despiked' plot of long wave radiation

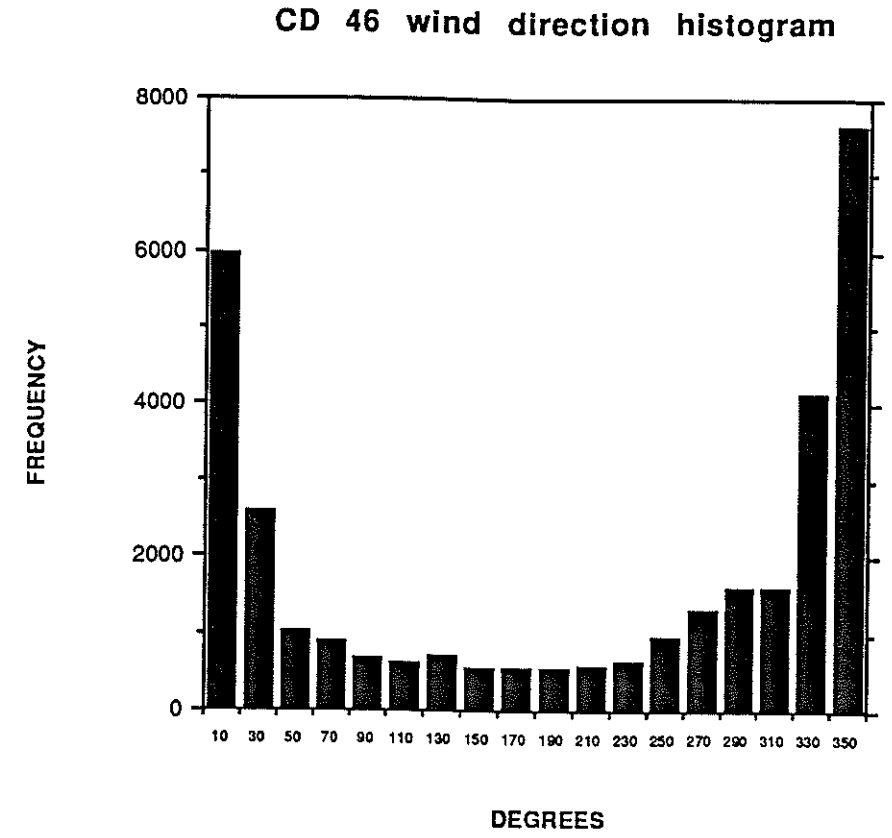

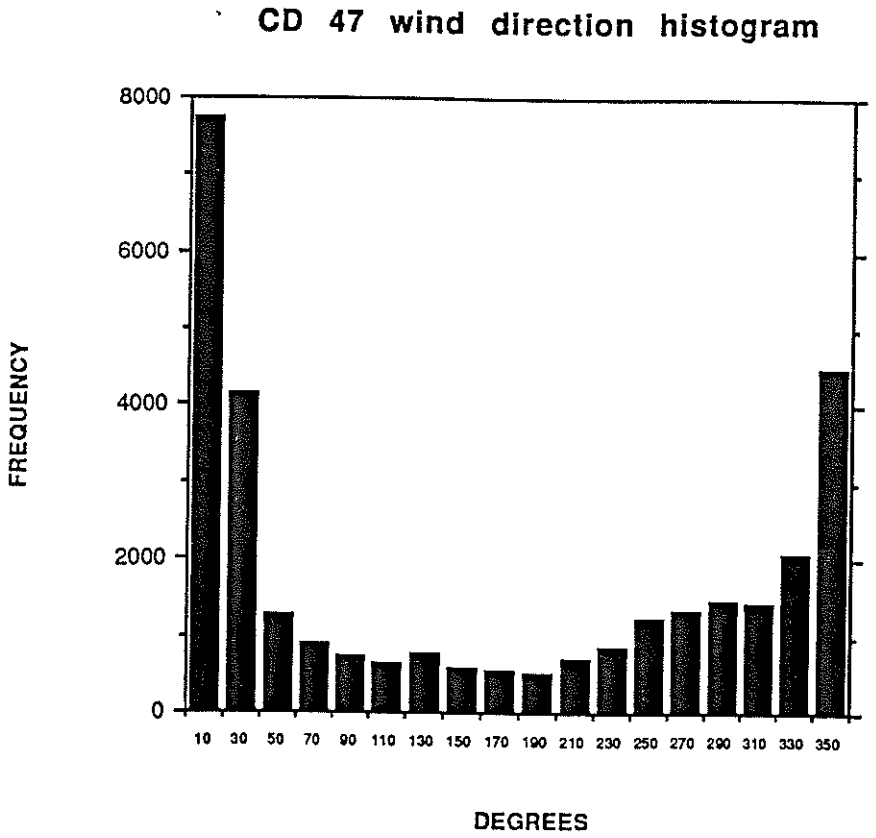

Fig 6 Histograms of wind direction for CD 46 and CD 47 showing the predominant wind direction is between 330° and 30°

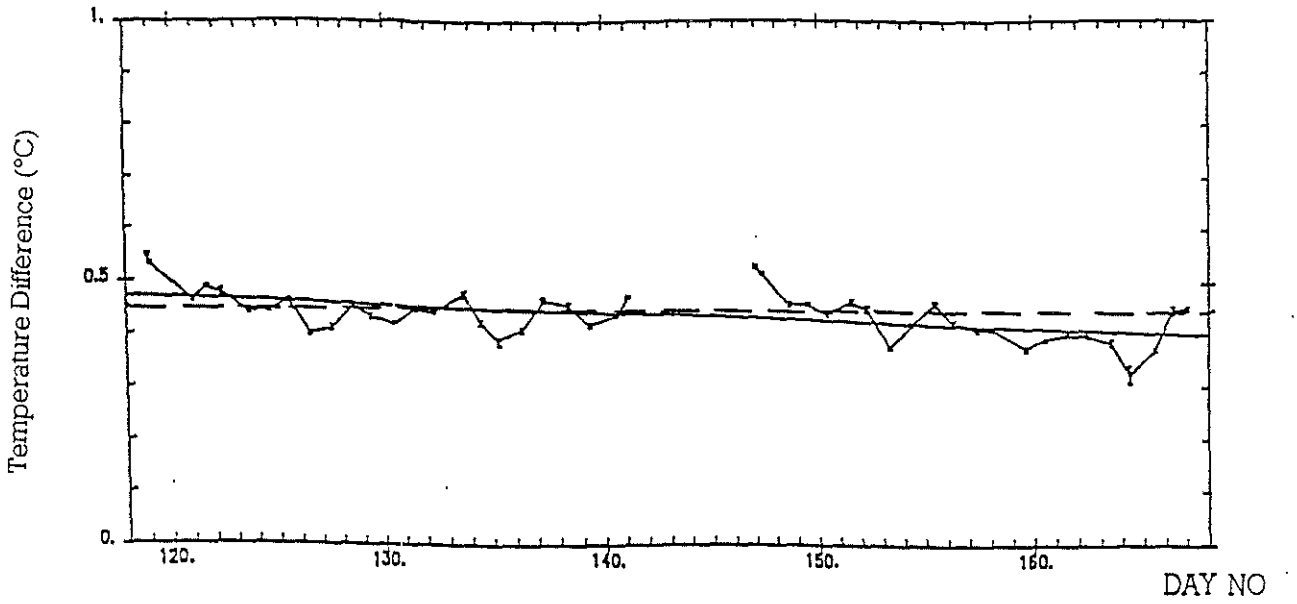

Fig 7 The differences between temperature readings from the psychrometers on the forward mast and those on the starboard for cruises CD46 and CD47 show a systematic negative trend, but overall changes were negligible (<0.1°C). The dashed line shows the recommended calibration correction.

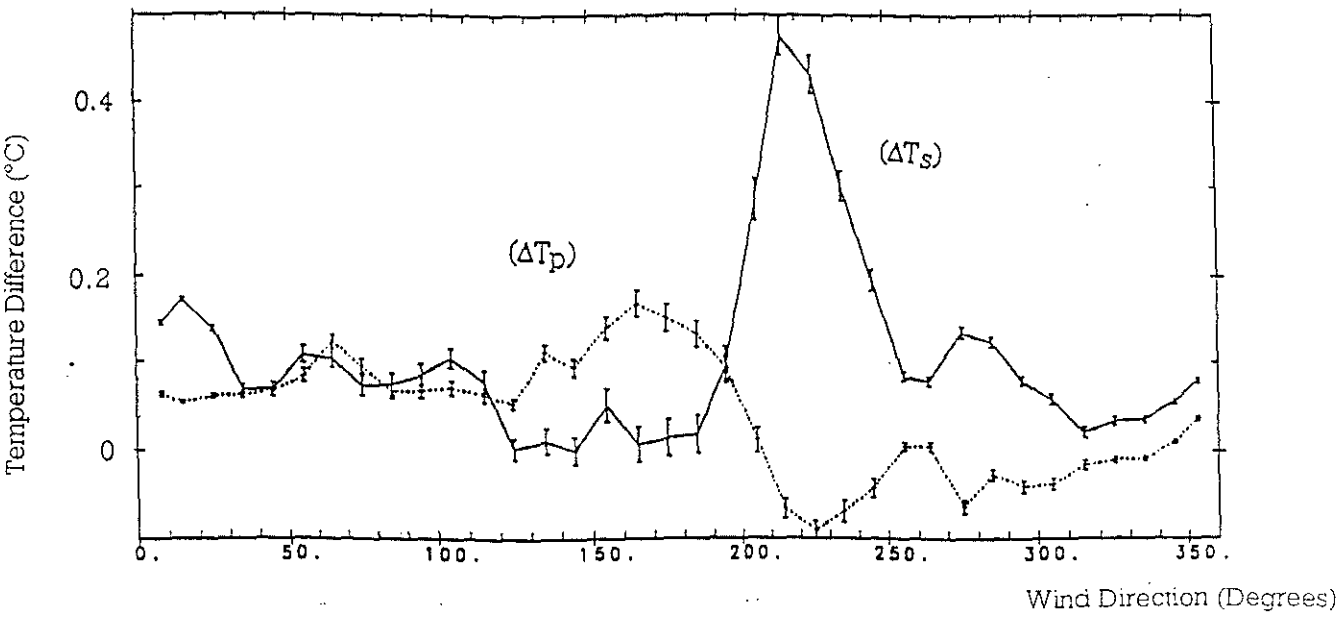

Fig 8 The differences between temperature readings from the psychrometers on the forward mast and those on the starboard (ΔT_S), and port masts (ΔT_P), relative to wind direction. The effect of funnel smoke is shown for the starboard psychrometer, for wind directions 200° to 250°.

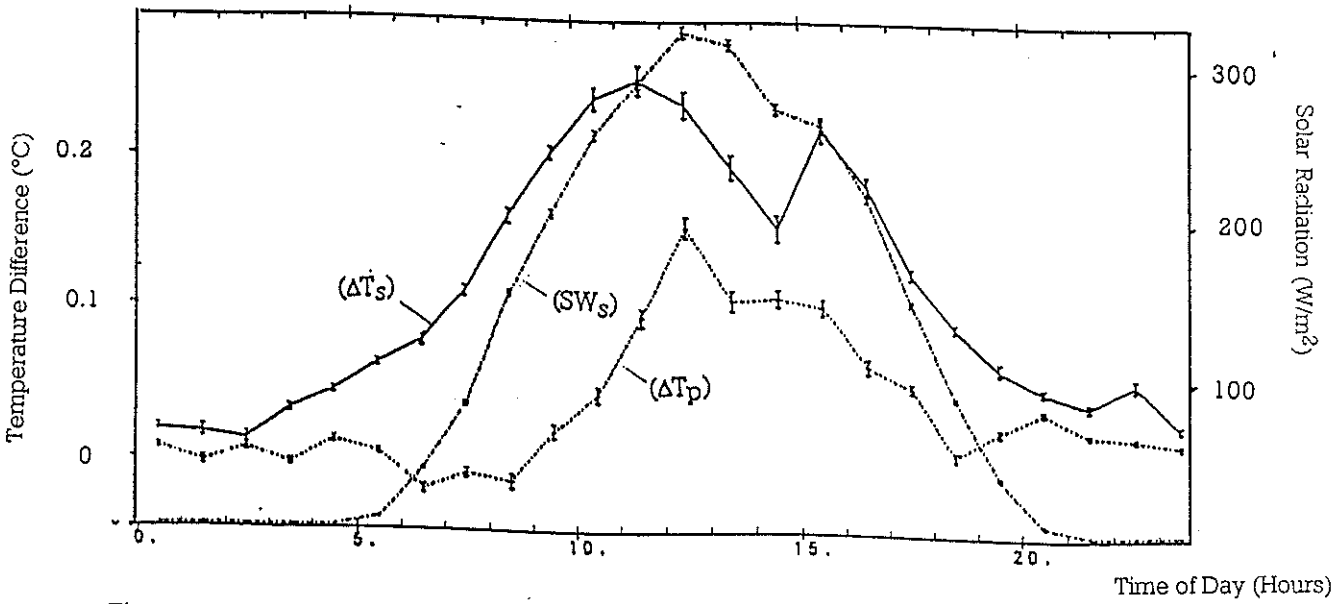

Fig 9 The mean diurnal variation of: incoming shortwave radiation (SW_S); temperature difference between dry bulb starboard and dry bulb forward psychrometers (ΔT_S); temperature difference between dry bulb port and dry bulb forward psychrometers (ΔT_P).

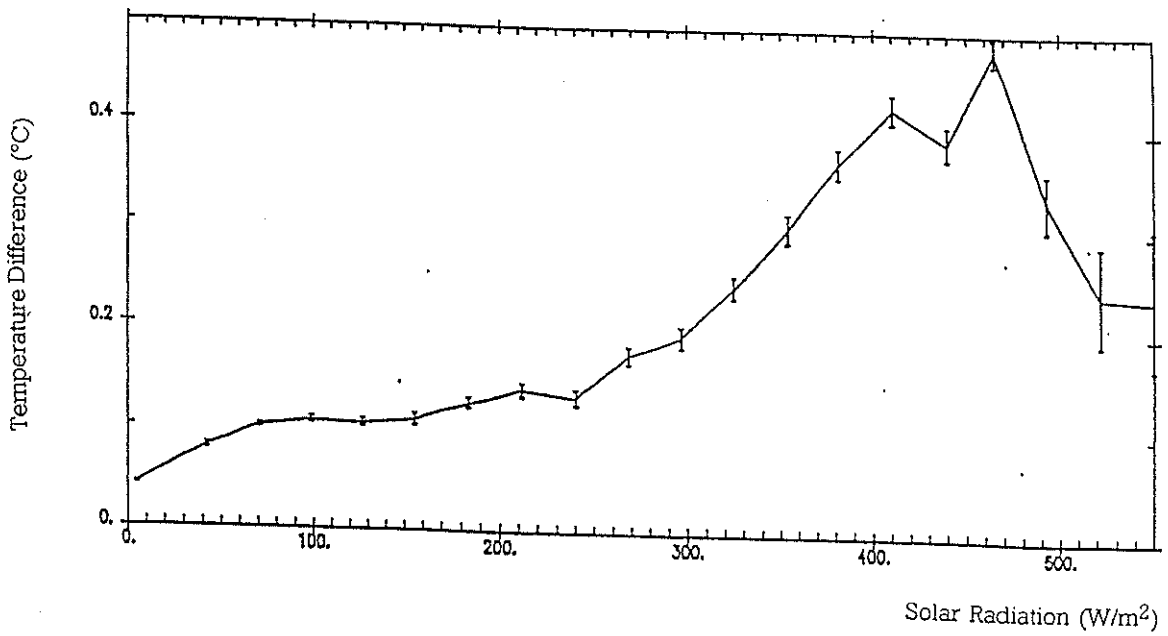

Fig 10 The difference between temperature readings from the psychrometers on the starboard mast and those on the forward mast, relative to short wave solar radiation.

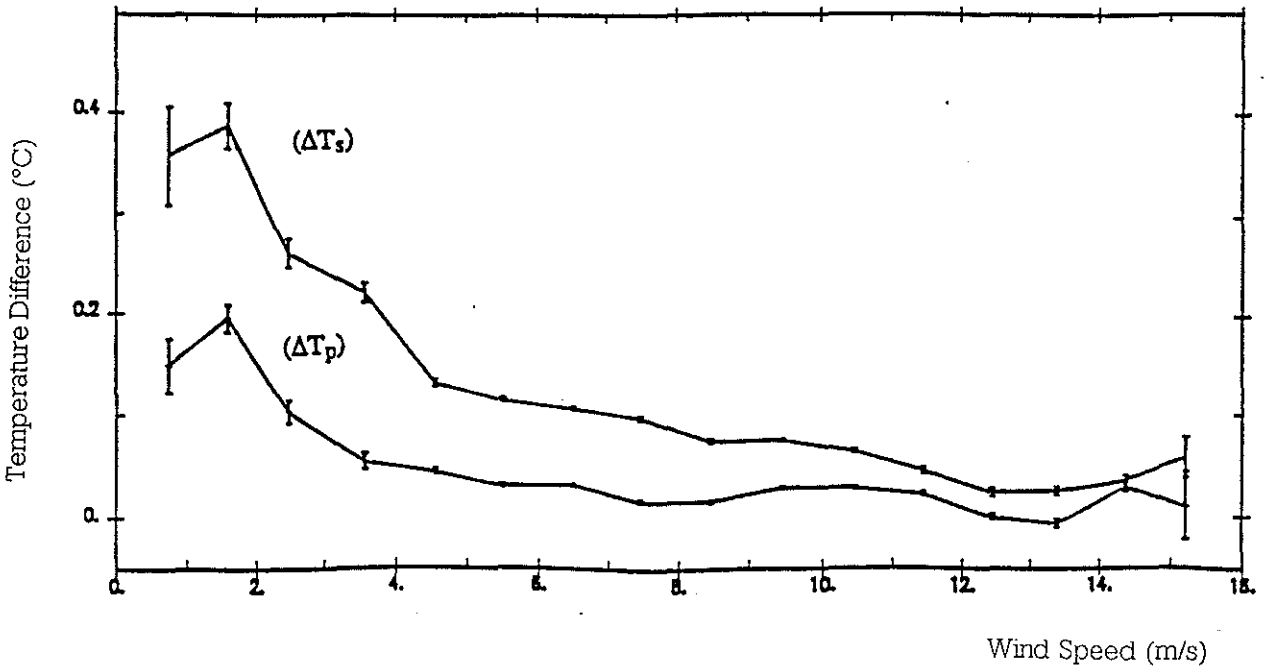

Fig 11 The difference between temperature readings from the psychrometers on the starboard (ΔT_S) and port masts (ΔT_P) and those on the forward mast, relative to all wind speeds.

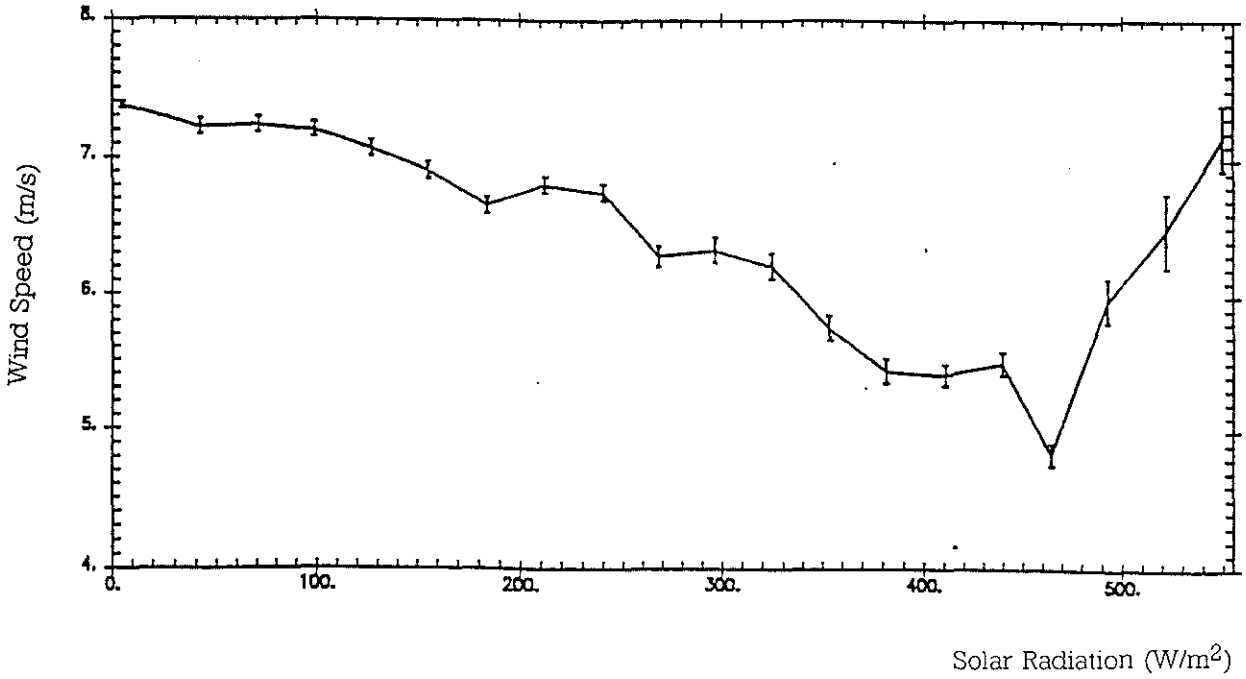

Fig 12 Mean wind speeds relative to incoming radiation, showing wind speed increases for high values of solar radiation.

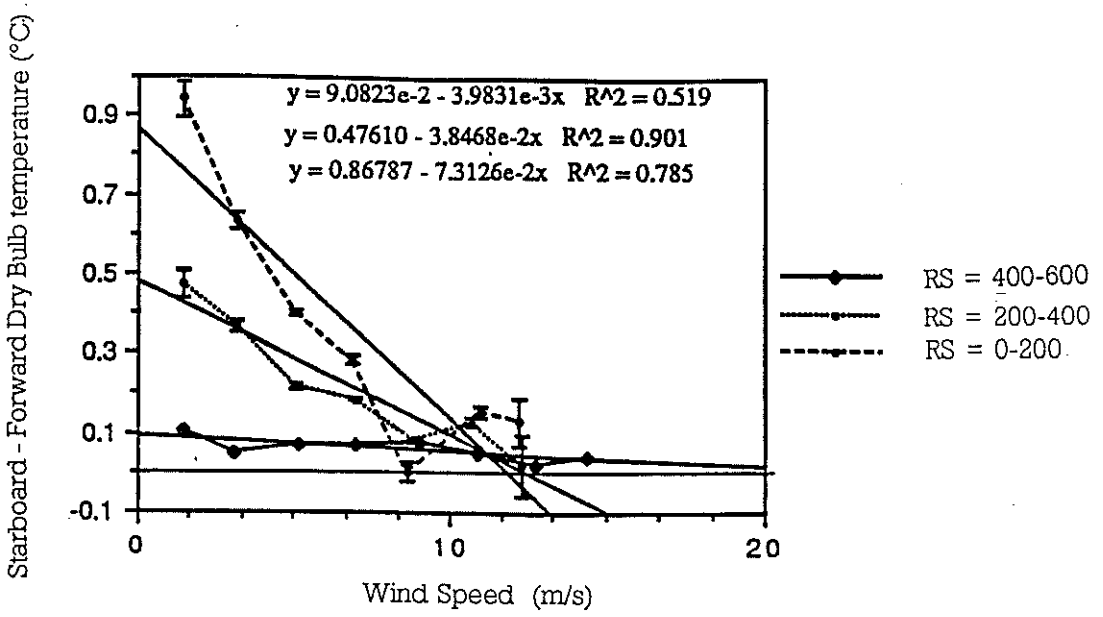

Fig 13a Regression plots of temperature difference against wind speed, for constant solar radiation values. The resulting gradients are used in Fig 14.

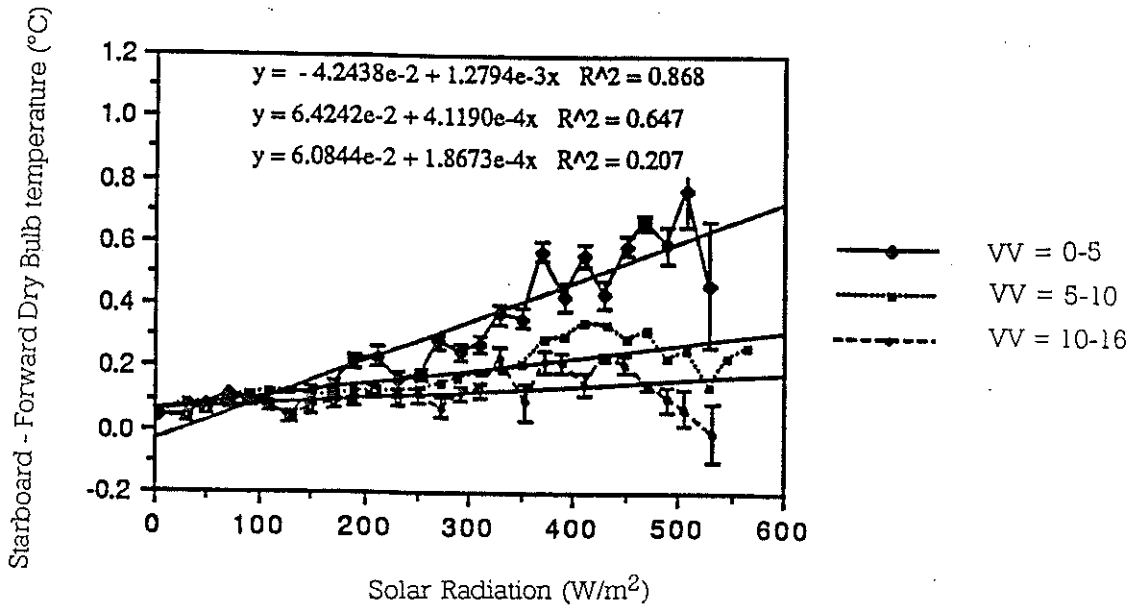

Fig 13b Regression plots of temperature difference against solar radiation, for constant wind speed values. The resulting gradients are used in Fig 15.

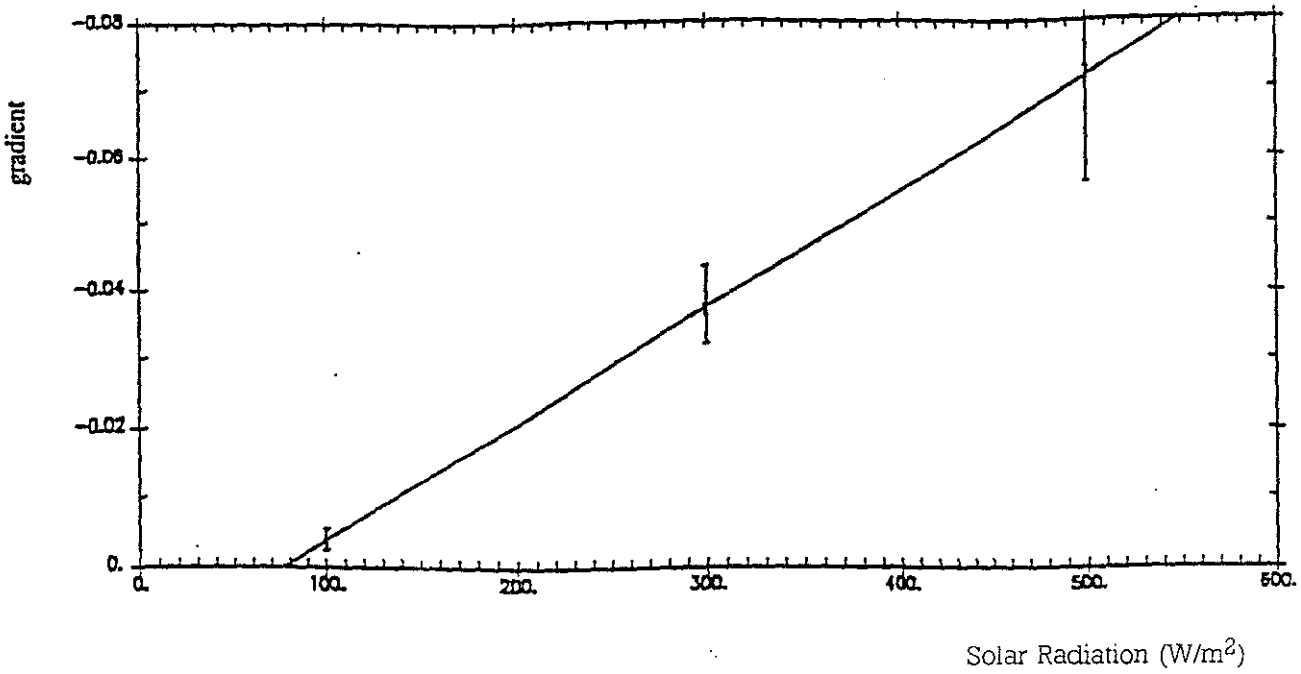

Fig 14 Regression plot of gradients from Fig 13a, against solar radiation, showing a strong linear relationship.

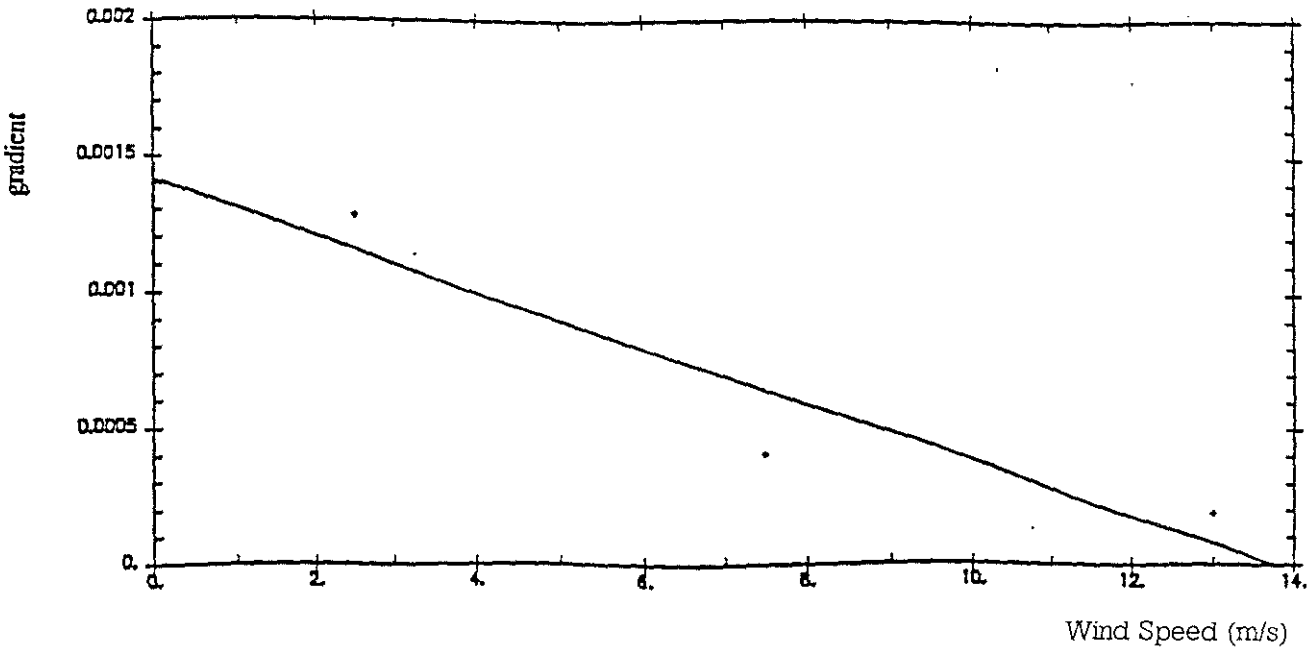

Fig 15 Regression plot of gradients from Fig 13b, against wind speed, the relationship is non linear.

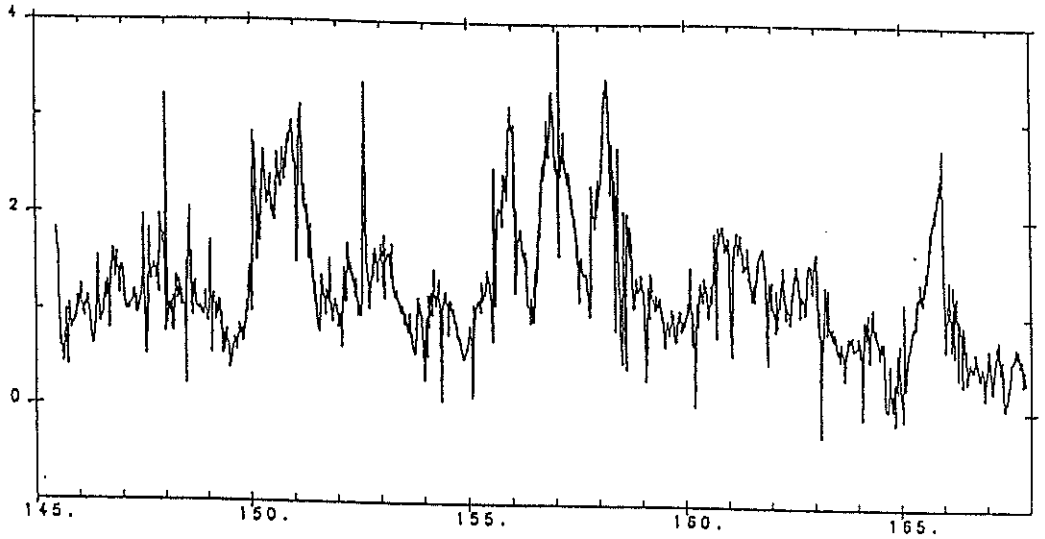

Fig 16 Time series of the difference between the anemometer readings from the main and forward masts

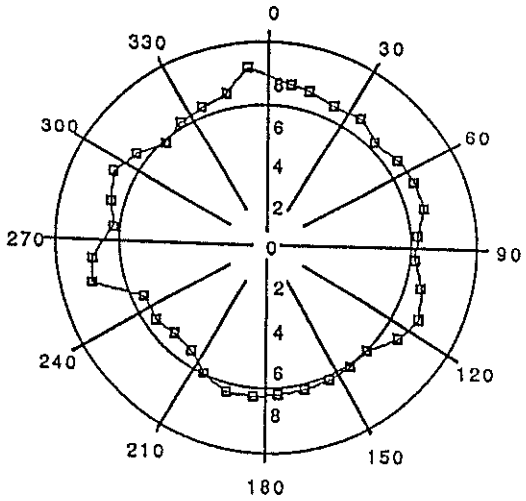

Fig 17 Radial plot of the main mast anemometer readings in m/s (after post cruise calibrations) as a function of wind direction; showing the mean wind speed for the whole cruise

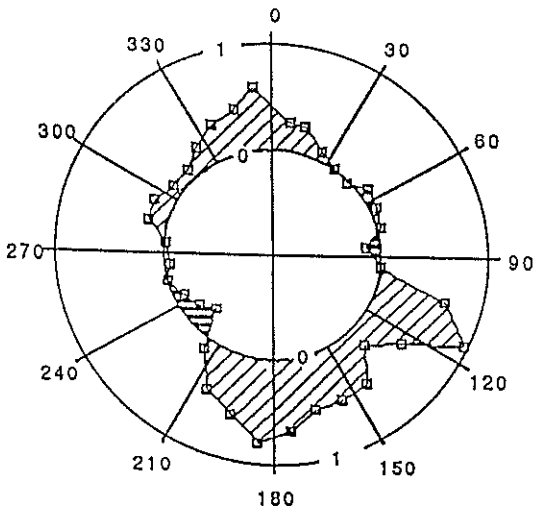

Fig 18 Radial plot of the differences in the anemometer readings (m/s) between the main and forward masts (after post cruise calibrations and height difference between the two anemometers have been accounted for) as a function of wind direction

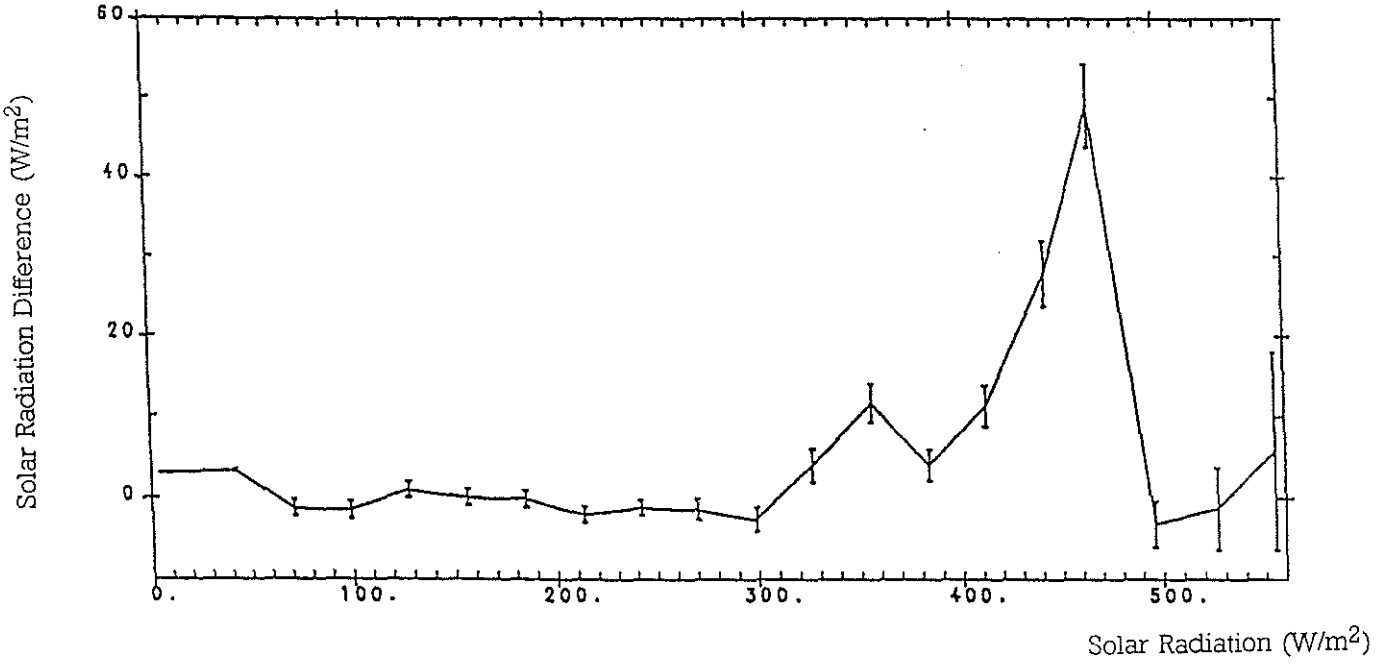

Fig 19 Difference between incoming solar radiation from the starboard and port sensors relative to the incoming solar radiation from the starboard sensor. When the incoming radiation is greater than 350 W/m^2, the port sensor reads lower than the starboard sensor.

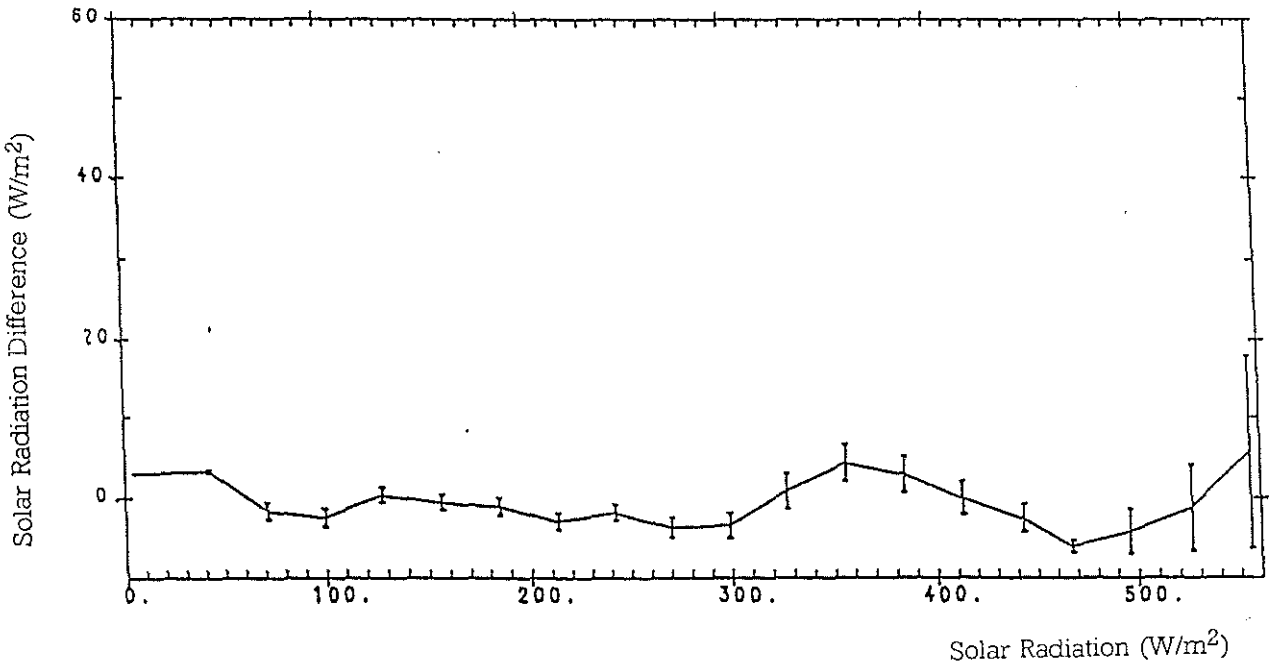

Fig 20 Difference between incoming solar radiation from the starboard and port sensors relative to the incoming solar radiation from the starboard sensor. Without data from day number 164 and 167

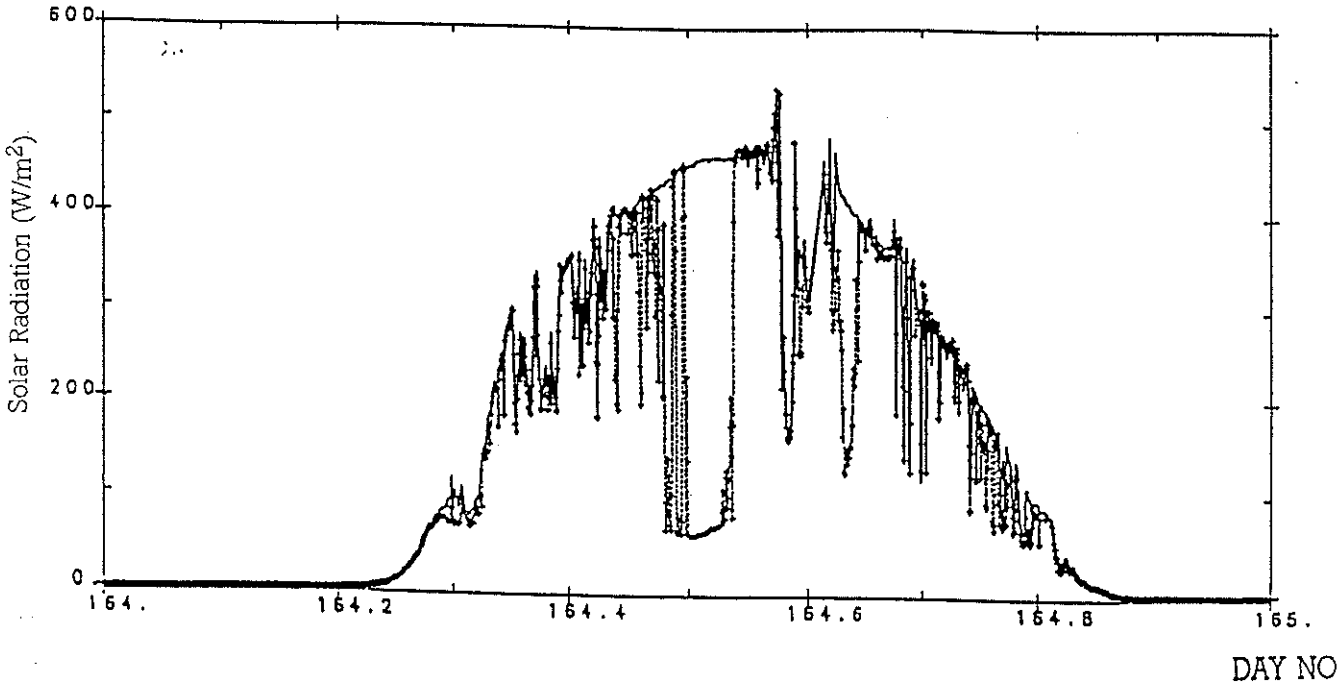

Fig 21 Plot of port and starboard incoming shortwave radiation for day number 164, showing the port reading lower than the starboard sensor

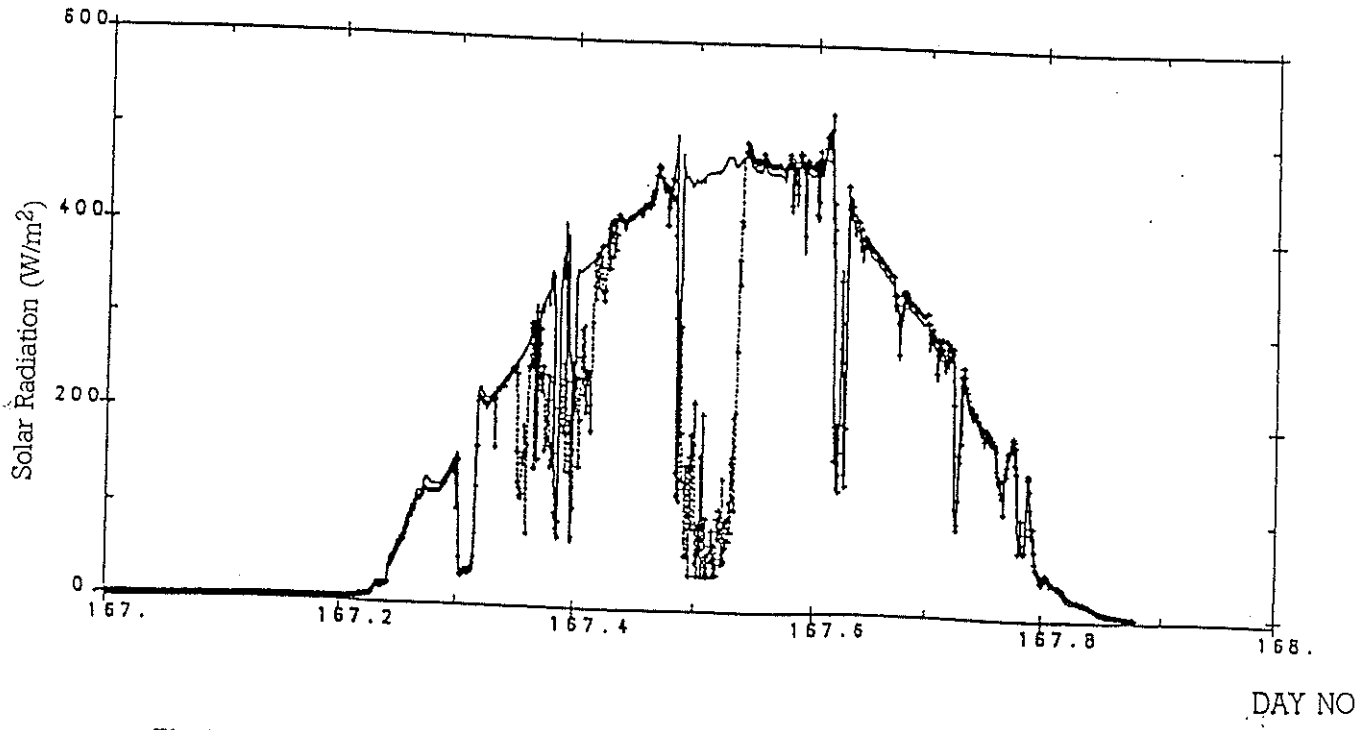

Fig 22 Plot of port and starboard incoming shortwave radiation for day number 167, showing the port reading lower than the starboard sensor

APPENDIX I: STATISTICAL ANALYSIS OF THE COMPARISON OF PSYCHROMETER READINGS

I.1 Statistical Analysis

Differences between temperature readings from the psychrometer on the forward mast and those on the wheelhouse top are expected to vary with relative wind direction, wind velocity, and solar heating. To determine the nature of this dependence a statistical model was developed for BOFS47 data, which investigated the correlation between one dependent variable (temperature difference between the dry bulb starboard psychrometer and the dry bulb forward psychrometer (ΔT_{SF})) and three independent variables; wind direction (DD), wind velocity (VV), and shortwave radiation (RS); in various combinations. The data was recorded at 1 Hz; 10 minute average values were calculated from the 1 Hz values for the following analysis.

I.1.1 Linear Model using Minitab

The first model used was a regression of ΔT_{SF} on all three available variables, fitted as:

$$\Delta T_{SF} = \alpha + \beta DD + \gamma VV + \varepsilon RS$$

where: ΔT_{SF} = dry starboard temperature - dry forward temperature, DD = wind direction, VV = wind velocity on the forward mast, RS = short wave solar radiation on the starboard sensor, $\alpha,\beta,\gamma,\varepsilon$ = constants

Table I.1 shows the correlation coefficients from regressing the above model using Minitab.

TableI.1: Correlation Coefficients (R value)

MODEL	R value
$\alpha DD+\beta VV+\gamma RS$	0.540
$\beta VV+\gamma RS$	0.534
$\alpha DD+\gamma RS$	0.523
$\alpha DD+\beta VV$	0.290

Examination of the r values concludes that excluding RS causes a considerable loss in the r value, and therefore the fit of the model. From the r values it can be seen that so long as the model contains RS, the model is worthy of analysis; so the two most significant models are:

$$\Delta T_{SF} = \alpha + \beta DD + \gamma VV + \varepsilon RS + \phi variable \qquad \text{(model A)}$$

$$\Delta T_{SF} = \alpha + \gamma VV + \varepsilon RS + \phi variable \qquad \text{(model B)}$$

Examination of the Minitab residual plots of the three variables (DD,VV,RS), indicated that the model could be further refined by the addition of terms in $VV^{1/2}$ (as the residual plot of VV tends to divergence) and/or RS^2 (as the residual of RS plot tends to convergence). Combinations of these variables were therefore added to the models A and B (ϕvariable in the above models). Table I.2 shows the correlation coefficients from regressing model A and model B, with the addition of combinations of $VV^{1/2}$ and RS^2.

Table I.2: Correlation Coefficients

MODEL USED		TERM	ADDED		
MODEL	NONE	$+VV^{1/2}$	$+RS^2$	$+VV^{1/2}+RS^2$	VV*RS
A	0.540	0.564	0.560	0.577	0.616
B	0.534	0.555	0.551	0.567	0.602
MODEL	VV*DD	RS*DD	VV^2	$RS^{1/2}$	$VV^{1/2}*RS^2$
A	0.542	0.540	0.550	0.559	0.548
B	0.539	0.534	0.539	0.550	0.539

The increase in the correlation coefficient obtained by the addition of wind direction in model A was not great enough to merit the addition of the parameter in the model. Also the plot of residuals against wind direction showed a random plot thus helping confirm this assumption. Thus from the results the best model was found to be:

$$\Delta T_{SF} = \alpha + \gamma VV + \varepsilon RS + \phi(VV*RS) \qquad \text{(model 1)}$$

(where: $\alpha = 0.0018$, $\beta = 0.00489$, $\varepsilon = 0.00178$, $\phi = -0.000175$)

But the r value for this model, even though it is the largest is still relatively small, and the model cannot be accepted. The increase in the r value for new models compared to the original model, is due to the addition of another parameter or combination of parameters, rather than a significantly better fit. The model explains 36.6 % of the variance, of which 1.8 % is explained by γVV, 5.1 % by α, 7.8 % by $\phi(VV*RS)$, and 21.9 % by εRS. Table I.3 shows the variance explained by each term by the best fit model (model 1).

Table I.3: Variance Explained by each Variable of Model 1

variable	variance
α	
$\alpha+\gamma VV$	6.8
$\alpha+\varepsilon RS$	26.9
$\alpha+\gamma VV+\varepsilon RS$	28.7
$\alpha + \gamma VV + \varepsilon RS + \phi(VV*RS)$	36.6

I.1.2 Non-Linear Model

The next stage was to attempt a non linear fit. After looking at plots of Δ_{SF} against VV, and also against RS, the plots showed an exponential tendency, so the following non linear model was tried:

$$\Delta T_{SF} = \alpha + \beta\exp(\gamma VV) + \delta\exp(\varepsilon RS)$$

where: $\alpha,\beta,\gamma,\delta,\varepsilon$ are constants of the regression

An IMSL program was used to find the values of the unknown constants, but the program did not converge to any values for the coefficients. This non-convergence does not constitute proof of the model being invalid, but it is a strong indication.

I.1.3 Analysis of smoothed data

From the data plots the data has an overall trend (envelope), and a diurnal variation. The problem is that the correlation could be due only to the diurnal variation, therefore the diurnal variation needs to be removed. So using a data file of hourly averaged data and executing a 24 point moving average on the data, the obtained result is a smooth envelope plot; the residuals (daily variation) can be found by the subtraction of the envelope data from the original input data. The envelope data can now be analysed to see if there is any correlation between the variables. This was implemented using a Fortran program, and Table I.4 shows the correlation coefficients from regressing the smoothed envelope data on model B using Minitab.

TableI.4: Correlation Coefficients (Envelope Data)

MODEL USED		TERM	ADDED		
	NONE	VV*RS	$V^{1/2}$	V^2	$V^{1/2}$*RS
B	0.622	0.703	0.704	0.699	0.713

The increase in the r value is due to the addition of another variable, as it is not a sufficiently large enough increase to warrant otherwise. Table I.5 shows the correlation coefficients from regressing the residual data on different models.

Table I.5: Correlation Coefficients (Residual Data)

MODEL USED		TERM	ADDED		
	NONE	VV*RS	V^2	COS(VV)	COS(RS)
B	0.577	0.586	0.579		
$\alpha+\gamma RS$				0.577	
$\alpha+\beta VV$					0.182

From the results, about 40% (r^2 value) of the original observed data was explained by a linear regression model containing shortwave radiation and wind speed (model 1). The smoothed envelope data (data with diurnal variation removed) gave a better correlation than the original data, as the short period variance (noisy data) had been smoothed out.

smoothed envelope data (data with diurnal variation removed) gave a better correlation than the original data, as the short period variance (noisy data) had been smoothed out.

I.1.4 Removal of funnel effect

The funnel of the ship causes warming of the starboard psychrometer. Table I.6 shows the correlation coefficients from regressing the envelope data with the funnel effect removed on model B.

Table I.6: Correlation Coefficients (Funnel Effect Removed)

MODEL USED	TERM ADDED	
	NONE	VV*RS
B	0.607	0.676

As can be seen from the above table, the removal of the funnel effect causes a decrease in the correlation coefficient. When the wind direction is aligned with the direction between the funnel and the starboard psychrometer, the funnel gases warm the instrument, thus introducing a strong and spurious correlation for that wind direction; removal of this effect causes the correlation coefficient to decrease.

I.1.5 Port Data

Using the port data instead of the starboard, and the following model:

$$\Delta T_{PF} = \alpha + \beta DD + \gamma VV + \delta RS + \phi variable \qquad \text{(MODEL C)}$$

where: ΔT_{PF} = dry port temperature - dry forward temperature, DD = wind direction, VV = wind velocity on the forward mast, RS = short wave solar radiation on the port sensor

Table I.7 shows the correlation coefficients from regressing the port data on different models.

Table I.7: Correlation Coefficients (Port Data)

MODEL	R
C	0.420
$\beta DD+\gamma VV$	0.268
$\beta DD+\delta RS$	0.416
$\gamma VV+\delta RS$	0.374

From the r value it is evident that again the exclusion of RS causes a considerable loss in the r value, and therefore the fit of the model. In this case it seems as though RS and DD are the most significant variables, rather than RS and VV, as with the starboard data. But, as previously mentioned, r values for these two models are very similar and thus either model is worthy of analysis.

APPENDIX II: PRE AND POST CRUISE CALIBRATION DETAILS FOR THE PSYCHROMETERS AND THE ANEMOMETERS

The following pre and post-cruise calibration coefficients are used in the equations in section 2.2.

II.1 Calibration Certificate for psychrometer VI1066 (Wet bulb foremast temperature) Date Produced : 01-18-1991

Pre- cruise		Post- cruise	
CAL	TW10190A	CAL	TW17190A
C(0)	-20.13991	C(0)	-22.31878
C(1)	3.41499E-04	C(1)	3.910506E-03
C(2)	9.100414E-06	C(2)	7.159736E-06
C(3)	4.265112E-10	C(3)	7.748193E-10

Table II.1: (Above) Calibration coefficients. (Opposite) Calculated temperatures and temperature differences from pre (A) and post-cruise (B) calibrations corresponding to the frequencies shown; also the overall mean temperature difference.

Freq	Temp A	Temp B	Diff
1400	-0.65	-0.68	0.03
1500	2.29	2.27	0.02
1600	5.45	5.44	0.01
1700	8.84	8.83	0.01
1800	12.45	12.44	0.01
1900	16.29	16.27	0.02
2000	20.36	20.34	0.02
2100	24.66	24.64	0.02
2200	29.20	29.19	0.01
2300	33.98	33.98	0.00
mean diff			0.01

II.2 Calibration Certificate for psychrometer VI1066 (Dry bulb foremast temperature) Date produced : 01-18-1991

Pre- cruise		Post- cruise	
Cal	TD10190B	CAL	TD17190A
C(0)	-21.59034	C(0)	-23.75074
C(1)	1.44664E-03	C(1)	4.959139E-03
C(2)	8.125E-06	C(2)	6.206677E-06
C(3)	4.861899E-10	C(3)	8.327876E-10

Table II.2: (Above) Calibration coefficients. (Opposite) Calculated temperatures and temperature differences from pre (A) and post-cruise (B) calibrations corresponding to the frequencies shown; also the overall mean temperature difference.

Freq	Temp A	Temp B	Diff
1400	-2.31	-2.36	0.05
1500	0.50	0.46	0.04
1600	3.52	3.48	0.04
1700	6.74	6.71	0.03
1800	10.17	10.14	0.03
1900	13.82	13.79	0.03
2000	17.69	17.66	0.03
2100	21.78	21.75	0.03
2200	26.09	26.07	0.02
2300	30.63	30.62	0.01
mean diff			0.03

II.3 Calibration Certificate for psychrometer VI1070 (Wet bulb starboard temperature) Date Produced : 01-18-1991

Pre- cruise		Post- cruise	
Cal	TW10190A	CAL	TW17190A
C(0)	-20.29832	C(0)	-22.99918
C(1)	-1.983848E-04	C(1)	4.490582E-03
C(2)	9.632186E-06	C(2)	6.991665E-06
C(3)	3.524534E-10	C(3)	8.399548E-10

Table II.3: (Above) Calibration coefficients. (Opposite) Calculated temperatures and temperature differences from pre (A) and post-cruise (B) calibrations corresponding to the frequencies shown; also the overall mean temperature difference.

Freq	Temp A	Temp B	Diff
1400	-0.73	-0.70	-0.03
1500	2.27	2.30	-0.03
1600	5.49	5.53	-0.04
1700	8.93	8.97	-0.04
1800	12.61	12.64	-0.03
1900	16.51	16.53	-0.02
2000	20.65	20.67	-0.02
2100	25.03	25.04	-0.01
2200	29.64	29.66	-0.02
2300	34.49	34.53	-0.04
mean diff			-0.03

II.4 Calibration Certificate for psychrometer VI1070 (Dry bulb starboard temperature)

pre- cruise		Post- cruise	
Cal	TD10190B	CAL	TD17190A
C(0)	-21.09177	C(0)	-23.5243
C(1)	-1.569352E-04	C(1)	3.944645E-03
C(2)	8.987747E-06	C(2)	6.778277E-06
C(3)	3.011681E-10	C(3)	6.873707E-10

Table II.4: (Above) Calibration coefficients. (Opposite) Calculated temperatures and temperature differences from pre (A) and post-cruise (B) calibrations corresponding to the frequencies shown; also the overall mean temperature difference.

Freq	Temp A	Temp B	Diff
1400	-2.87	-2.83	-0.04
1500	-0.09	-0.04	-0.05
1600	2.90	2.96	-0.06
1700	6.10	6.15	-0.05
1800	9.50	9.55	-0.05
1900	13.12	13.16	-0.04
2000	16.96	16.98	-0.02
2100	21.00	21.02	-0.02
2200	25.27	25.28	-0.01
2300	29.76	29.77	-0.01
mean diff			-0.03

II.5 Calibration Certificate for psychrometer VI1071 (Wet bulb port temperature)
Date Produced : 01-18-1991

Pre- cruise		Post- cruise	
Cal	TW10190A	CAL	TW17190A
C(0)	-21.29737	C(0)	-23.09244
C(1)	1.652338E-03	C(1)	4.886202E-03
C(2)	8.657969E-06	C(2)	6.813306E-06
C(3)	4.963314E-10	C(3)	8.365507E-10

Table II.5: (Above) Calibration coefficients. (Opposite) Calculated temperatures and temperature differences from pre (A) and post-cruise (B) calibrations corresponding to the frequencies shown; also the overall mean temperature difference.

Freq	Temp A	Temp B	Diff
1400	-0.65	-0.60	-0.05
1500	2.34	2.39	-0.05
1600	5.54	5.59	-0.05
1700	8.97	9.02	-0.05
1800	12.62	12.66	-0.04
1900	16.50	16.53	-0.03
2000	20.61	20.63	-0.02
2100	24.95	24.96	-0.01
2200	29.53	29.54	-0.01
2300	34.34	34.37	-0.03
mean diff			-0.03

II.6 Calibration Certificate for psychrometer VI1071 (Dry bulb port temperature)
Date Produced : 01-18-1991

Pre- cruise		Post- cruise	
Cal	TD10190B	CAL	TD17190A
C(0)	-20.93618	C(0)	-23.67878
C(1)	8.259702E-04	C(1)	5.227892E-03
C(2)	8.380603E-06	C(2)	6.058437E-06
C(3)	4.365153E-10	C(3)	8.404015E-10

Table II.6: (Above) Calibration coefficients. (Opposite) Calculated temperatures and temperature differences from pre (A) and post-cruise (B) calibrations corresponding to the frequencies shown; also the overall mean temperature difference.

Freq	Temp A	Temp B	Diff
1400	-2.16	-2.18	0.02
1500	0.63	0.63	0.00
1600	3.63	3.64	-0.01
1700	6.83	6.85	-0.02
1800	10.25	10.26	-0.01
1900	13.88	13.89	-0.01
2000	17.73	17.73	-0.00
2100	21.80	21.80	-0.00
2200	26.09	26.09	-0.00
2300	30.61	30.62	-0.01
mean diff			0.00

II.7 Calibration Certificate for anemometers VI1892 (Main mast anemometer) Date Produced : 01-24-1991

Pre- cruise		Post- cruise	
CAL	WS140789	CAL	WS13090A
C(0)	0.3840709	C(0)	0.2337457
C(1)	1.187526	C(1)	1.142083

TABLE II.7: (Above) Calibration coefficients. (Opposite) Calculated wind speeds and wind speed differences from pre (A) and post-cruise (B) calibrations corresponding to the frequencies shown; also the overall mean wind speed difference.

Freq	vel A	vel B	Diff
1	1.57	1.38	0.19
4	5.13	4.80	0.33
7	8.70	8.23	0.47
10	12.26	11.66	0.60
13	15.82	15.08	0.74
16	19.39	18.51	0.88
19	22.95	21.93	1.02
22	26.51	25.36	1.15
25	30.07	28.79	1.28
28	33.64	32.21	1.43
mean diff			0.81

II.8 Calibration Certificate for anemometers YG6992 (Forward mast propeller vane anemometer (Young)) Date Produced : 01-24-1991

Pre- cruise		Post- cruise	
Cal	WW13090A	CAL	WW34090A
C(0)	0 9.267765E-02	C(0)	8.143723E-02
C(1)	9.839436E-02	C(1)	9.852437E-02

TABLE II.8: (Above) Calibration coefficients. (Opposite) Calculated wind speeds and wind speed differences from pre (A) and post-cruise (B) calibrations corresponding to the frequencies shown; also the overall mean wind speed difference.

Freq	vel A	vel B	Diff
1	0.19	0.18	0.01
4	0.49	0.48	0.01
7	0.78	0.77	0.01
10	1.08	1.07	0.01
13	1.37	1.36	0.01
16	1.67	1.66	0.01
19	1.96	1.95	0.01
22	2.26	2.25	0.01
25	2.55	2.55	0.00
28	2.85	2.84	0.01
mean diff			0.01